Research article

Fluid flow and polymetallic sulfide mineralization in the Kettara shear zone (Jebilet Massif, Variscan Belt, Morocco)

I. N'Diaye[1], A. Essaifi[1,*], M. Dubois[2], B. Lacroix[3], K. M. Goodenough[4], L. Maacha[5]

[1]*Geology Department, Cadi Ayyad University, B.P. 2390, Marrakech 40000, Morocco*

[2]*LGCgE (EA 4515) / Université Lille 1, building SN5, 59655 Villeneuve d'Ascq CEDEX, France*

[3]*Institut des Sciences de la Terre, Université de Lausanne, 1015 Lausanne, Switzerland*

[4]*British Geological Survey, Murchison House, West Mains Road, Edinburgh EH9 3LA, UK*

[5] *Managem group, BP5199, Casablanca, 20100 Morocco*

*Corresponding author: Abderrahim Essaifi

email: essaifi@uca.ma

Tel +212 5 24 43 46 49 (work) +212 5 24 49 05 61 (home) Fax +212 5 24 43 74 11

Abstract

The Kettara shear zone is a regional wrench shear zone within the Jebilet massif of Western Morocco, part of the Variscan orogenic belt. This massif is characterized by bimodal magmatism, largely intrusive, and by a number of polymetallic massive sulfide deposits. A syntectonic mafic-ultramafic intrusion and an adjacent, deformed pyrrhotite-rich massive sulfide deposit are located within a 'compressional jog' of the shear zone. Hydrothermal alteration in both the intrusion and the wall rocks adjacent to the deposit is characterized by syntectonic replacement processes leading to formation of chlorite-schists and quartz ± calcite veins. Fluid inclusions in mineralized (pyrrhotite-bearing) quartz veins from the wall rocks adjacent to the deposit and in veins associated with chlorite-schists within the intrusion indicate a prevalence of H_2O-CO_2-CH_4-N_2 and H_2O-salt fluid systems. In the mineralized veins the fluid shows reducing conditions, with gas dominated by CH_4 and N_2 and salinities around 7.5 wt.% NaCl, whereas in the chlorite shear zones fluid is CO_2 dominated and salinities are higher than 23 wt.% NaCl. Hydrogen and oxygen isotopic compositions of chlorite and quartz are similar and demonstrate involvement of metamorphic water in both the deposit and the intrusion.

The data are consistent with a regional metamorphic fluid flow through the Kettara shear zone. The migrating metamorphic fluids were reduced in the organic matter-rich host rocks leading to deposition of sulfides in the mineralized veins. There are two possible hypotheses for the origin of these mineralized veins: either they were formed during deformation and remobilization of a syn-sedimentary massive sulfide deposit, or they were formed synchronously with the sulfide deposit during development of the Kettara shear zone.

Keywords Kettara · Shear zones ·Massive sulfide deposits · Stable isotopes · Fluid inclusions · Variscan Belt · Morocco

1. Introduction

Crustal shear zones form narrow zones of low strength and high permeability within the upper crust, and may serve as fluid pathways, capable of focusing ore-forming processes (Oliver, 1996; Cox et al., 2001; Chernicoff et al., 2002). The association of many hydrothermal mineral deposits with shear zones and crustal discontinuities is widely documented in the literature (e.g., Groves et al., 1998; Sillitoe, 2000). Examples of mineralization that display a spatial relationship with fault and shear zones include orogenic gold deposits (e.g., Sibson et al., 1988; Cox et al., 1991; Bouchot et al., 2000). Polymetallic sulfide mineralization associated with shear zones has been described at a range of structural levels (Glen, 1987; Nicol et al., 1997; Gaouzi et al., 2001; Piessens et al., 2002; Bellot, 2004) and emphasizes the importance of this type of mineralization in collisional belts. Hydrothermal fluid flow associated with syntectonic intrusions may be concentrated along shear zones and, when combined with a precipitation mechanism operating in a restricted space (e.g., Hedenquist and Lowenstern, 1994), may lead to ore deposition. This work focuses on a shear zone hosting a mafic-ultramafic intrusion and a massive sulfide deposit in the Variscan belt of Morocco, and considers the relationship between deformation, fluid flow and sulfide mineralization.

The central unit of the Jebilet massif, in the Marrakech region of Western Morocco, is a block of Carboniferous sedimentary rocks deformed during the Variscan orogeny. The block is located along the southern branch of the West Meseta shear zone (Piqué et al., 1980; Lagarde and Michard, 1986). This block and its southern extension (the Guemassa massif) host a bimodal intrusive magmatic suite (Bordonaro, 1983; Essaifi et al., 2014) and significant massive sulfide mineralization (Huvelin, 1972; Bernard et al., 1988). The origin of the massive sulfide deposits is the subject of continuing debate. They have been variously considered as deformed syngenetic VMS or SEDEX bodies (Belkabir et al., 2008; Marcoux et al., 2008; Moreno et al., 2008; Lotfi et al., 2008) or as later syntectonic bodies (Essaifi and Hibti, 2008).

The Kettara deposit is a pyrrhotite-rich, near-vertical massive sulfide lens located near the mafic-ultramafic Kettara intrusion. Both are located within a shear zone interconnected with a regionally anastomosing network of sub-vertical shear zones (Essaifi et al., 2001; Essaifi and Hibti, 2008).The deposit has previously been interpreted as a mineralized dyke filling a sub-vertical fracture (Agard et al., 1952), or as a deformed pre-tectonic, synsedimentary deposit (Huvelin, 1970).

The Kettara deposit was the first massive sulfide deposit to be discovered and mined in central Jebilet. The gossan was exploited for limonite and ochre from 1938–1963. The extracted quantities are 150 000 t grading 45–52% Fe and 50 000 t grading 50–58 % Fe, respectively (Essaifi, 2011 and references therein). Below the gossan a cementation zone with mineralization composed of native copper, pyrite, chalcocite (Cu2S), covellite (CuS), with traces of gold and silver (Souaré, 1988) is present. Pyrite was extracted from this zone between 1955 and 1966, and used in the manufacture of sulfuric acid with recuperation of Cu contained in chalcocite and covellite. Its total reserves have been estimated as 180 000 t grading 38% sulfur. Below the cementation zone, the primary mineralization is pyrrhotite-rich (up to 95%) and forms an elongate sub-vertical lens 500 m deep, 40–70 m thick and 1500 m long (Huvelin and Permingeat, 1980; Bernard et al., 1988). The ore reserves are estimated as 30 Mt of pyrrhotite grading 0.7% Cu; with 8 Mt extracted between 1964 and 1982, and used in the manufacture of sulfuric acid. Difficulties related to pyrrhotite storage (fast oxidation), poor sulfur content (25%), and to the volume of mine wastes resulted in the closure of the operation in 1982.

This paper presents new structural, chemical and fluid inclusion evidence of regional fluid migration along the Kettara shear zone, leading to synkinematic hydrothermal alteration around the polymetallic sulfide mineralization, and discusses the significance of this fluid migration on the genesis of the Kettara massive sulfide deposit.

2. Geological Framework

2.1. The Moroccan Meseta

The Variscan orogenic belt of Morocco is subdivided into the eastern and western Meseta domains (Fig. 1A, B), which were folded and metamorphosed respectively during late Devonian and late Carboniferous (mainly early Westphalian) Variscan tectonic events (Hollard, 1978; Hoepffner et al., 2005; Michard et al., 2010). The Jebilet massif, together with the Rehamna and the central Paleozoic massifs to the north, and the high Atlas Paleozoic block to the south, form the Western Meseta. A late Devonian-early Carboniferous foreland sedimentary basin was developed in the western Meseta and was bounded by relatively rigid blocks to the north (Sehoul block) and west (Coastal block) and by the Anti-Atlas and West African craton to the south (Piqué and Michard, 1989; Hoepffner et al., 2006; Burkhard et al., 2006). Basin closure during the late Carboniferous was accompanied by strongly heterogeneous ductile deformation. Narrow, highly deformed regional shear zones of low to medium metamorphic grade contrast with wide moderately deformed areas with very low-grade metamorphism (Piqué et al., 1980, Lagarde and Michard, 1986; Piqué and Michard, 1989). The narrow deformed zones and are commonly spatially associated with syn- to late-kinematic granitic intrusions (Lagarde et al., 1990). Among these shear zones, the western boundary of the Devonian-Carboniferous basin is a major lithospheric structure, the West Meseta Shear Zone (WMSZ), which extends from Rabat in the north to the High Atlas in the south (Piqué et al., 1980; Lagarde and Michard, 1986). Most geodynamic models relate formation of the Moroccan Meseta to a westward continuous compression of the Variscan foreland in which the Rheic suture is hidden at the eastern boundary of the eastern Meseta

(Kharbouch et al., 1985; Boulin et al., 1988; Roddaz et al., 2002, 2006; Essaifi et al., 2014). Recent structural and geochronological work in the Rehanma Massif by Chopin et al. (2014) indicates a more complex (polyphase) history beginning with southward thrusting, followed by N-S directed bulk crustal shortening, in turn followed by E-W crustal shortening, all occurring from late Carboniferous to Lower Permian times.

2.2. The Jebilet massif

The Jebilet massif, just north of Marrakech provides an E-W section through the western Meseta domain. It is composed of three structural units (Fig. 1C):

i) The western Jebilet unit is a weakly deformed block composed of unmetamorphosed Cambro-Ordovician limestones, shales and sandstones with north-south trending kilometer-scale folds. It is part of the Coastal block, which was emergent since Devonian times (Piqué et al., 1980).

(ii) The central Jebilet unit consists of a schistose low-grade metamorphosed (anchizone and epizone) block of marine Visean shales (the Sarhlef schists) deposited in an anoxic platform setting (Beauchamp, 1984). This unit is also characterized by the occurrence of massive sulfide deposits together with numerous magmatic mafic and felsic intrusions which form a bimodal magmatic association (Bordonaro, 1983; Essaifi et al., 2014). The boundary between the central and western Jebilet is a NNE–SSW dextral thrust-wrench shear zone (Le Corre and Bouloton 1987; Mayol and Muller, 1985), and this is the southern extension of the West Meseta Shear Zone (WMSZ, Fig. 1B, C).

(iii) The eastern Jebilet unit is a weakly metamorphosed to unmetamorphosed block separated from the central unit by a sinistral shear zone with a NNW-SSE trend, the Marrakech Shear Zone (Lagarde and Choukroune, 1982). It is composed of Upper Visean syntectonic ‘flysch’ (Kharrouba flysch) including olistostromes and inliers of Ordovician to Devonian sedimentary rocks. Such Carboniferous syntectonic deposits also characterize the eastern part of central Morocco and were deposited in a compressional retro-foreland basin (Bouabdelli and Piqué, 1996; Ben Abbou et al., 2001; Roddaz et al., 2002).

Two syntectonic calc-alkaline granite plutons intruded by leucogranite sheets are spatially associated with the Marrakech shear zone (Lagarde and Choukroune, 1982). Westphalian-Permian continental conglomerates (Huvelin 1977) rest unconformably upon the Variscan folded sequence in western and eastern Jebilet (Fig. 1C).

3.3. Central Jebilet

The intersection of the SSE-oriented Marrakech Shear Zone with the major NNE-trending WMSZ delimits a trapezoidal block (central Jebilet) where the metasedimentary rocks have been deformed during a very low- to low-grade greenschist facies regional metamorphism contemporaneous with post-Visean shortening (Piqué and Michard, 1989; Hoepffner et al., 2005; Michard et al., 2010). Regional ductile deformation is marked by the development of a widespread subvertical axial plane schistosity (S_1) associated with NE–SW-trending, large-scale upright and subhorizontal folds. The schistosity trajectories progressively curve into an array of anastomosing shear zones (Fig. 2A), accompanied by increasing strain and metamorphic grade. These shear zones show a close spatial association with the bimodal intrusions and rotate anticlockwise by about 90° into the SSE trending Marrakech Shear Zone. These ductile shear zones evolve laterally into brittle faults that cut the schistosity. The most important of these is the Mesret dextral fault (Fig. 1C). Greenschist facies regional metamorphism during foliation development is indicated by white mica, chlorite, albite and quartz.

Carboniferous magmatism in the central Jebilet is dominated by intrusive rocks and includes a tholeiitic-alkaline bimodal association and two calc-alkaline cordierite-bearing granodioritic plutons intruded by leucogranite sheets (Le Corre and Saquaque, 1987; Mrini et al., 1992;

Essaifi et al., 2014). The bimodal intrusions are limited to the central Jebilet block, and the granodioritic plutons are spatially associated with the Marrakech Shear Zone (Fig. 1C).

The bimodal association (two-thirds mafic compositions, the remainder felsic) is syn-tectonic and was emplaced at 330.5 ± 0.7 Ma (Essaifi et al., 2003) at high crustal levels. The granodioritic plutons were also emplaced at c. 330 Ma, but the cross-cutting leucogranite sheets were intruded at c. 300 Ma (Mrini et al., 1992). The bimodal magmatic association is dominated by intrusive rocks forming dykes, small stocks and elongated intrusions of a few hundred meters width and a few kilometers length. The bimodal magmatic rocks are arranged into N–S- to NE–SW-trending lineaments that are broadly parallel to local schistosity and shear zones (Fig. 2A). Intrusion of these magmatic pods resulted in low-pressure contact metamorphism of the surrounding pelites, reaching the hornblende hornfels facies, and their emplacement was accompanied by significant hydrothermal activity (Essaifi, 1995).

The massive sulfide deposits of the Moroccan Meseta are restricted to the central Jebilet block and its southern extension, the Guemassa massif. They are Cu and Pb-Zn massive sulfide deposits dominated by pyrrhotite (Huvelin, 1970; Bernard et al., 1988; Essaifi and Hibti, 2008). In the central Jebilet, the deposits are steeply dipping elongate lenses aligned broadly parallel to the general trend of the regional structures (folds, schistosity) (Fig. 2A). Locally the deposits cut at a low angle across the regional schistosity and the mafic dykes of the bimodal magmatic association (Huvelin, 1972). At regional-scale the ore bodies and their gossans form north-south to NE-SW near-vertical lineaments, parallel with the bimodal magmatic lineaments, and they are generally located at a constant distance (~ 1 to 1.5 km) from the bimodal intrusions (Bernard et al., 1988; Essaifi and Hibti, 2008). The Kettara intrusion lies within one such magmatic lineament (Fig. 2). Two massive sulfide deposits in the area are currently mined: the Draa Sfar deposit on the southern margin of the central Jebilet block (Belkabir et al., 2008; Marcoux et al., 2008; Moreno et al., 2008), and the Hajjar deposit (Leblanc, 1993; Hibti and Marignac, 2001) in the Guemassa massif, some 30 km to the south. The Koudiat Aïcha deposit close to Kettara has also been the subject of recent study (Lotfi et al., 2008; 2010).

The sulfide bodies have not been directly dated. Hydrothermal alteration in the Hajjar sulfide deposit has been dated at c. 300 Ma, and attributed to proximity to a buried leucogranitic intrusion (Watanabe, 2002). In contrast, hydrothermal alteration associated with the Draa Sfar deposit is dated at c. 331 Ma (Marcoux et al., 2008), within error of the age of the bimodal intrusions.

2.4. The Kettara area

The Kettara mafic-ultramafic intrusion, located 1 km to the south of the Kettara massive sulfide deposit (Fig. 2), is a stratified intrusion composed of medium- to coarse-grained mafic and ultramafic cumulates, surrounded by a narrow zone of fringing microgabbros at the contact with the host rocks (Aarab, 1984; Jadid, 1989; Essaifi, 1995). The magmatic minerals consist of olivine, clinopyroxene, plagioclase, spinel, ilmenite and apatite. The ultramafic cumulates (plagioclase-bearing wehrlites, troctolites and olivine-bearing gabbros) are cross-cut by mafic cumulates (massive and layered leucogabbros), and enclaves of troctolites are found within leucogabbros. Numerous near-vertical felsic and mafic dykes cut across the intrusion and the host rocks (Fig. 2B, C and Fig. 3). Studies of the finite strain field and petrostructural analysis have demonstrated a syn-tectonic emplacement of the Kettara intrusion, which is transected by a series of anastomosing cm- to m-scale shear zones (Ait-Tahar, 1987; Essaifi et al., 2004). The intrusion lies within the Oled Har-Kettara_Safsafat magmatic lineament (Fig. 2B).

The Kettara sulfide deposit forms an elongated sub-vertical, pyrrhotite-dominated massive sulfide lens, approximately 1.5 km long and 500 m deep, parallel to the NE-SW regional structural trend (Essaifi and Hibti, 2008), and indicated at the surface by a well-developed gossanous zone up to 50 m in width (Fig. 2). It crops out approximately one kilometer north of the mafic-ultramafic Kettara intrusion (Fig. 2).

The host rocks of the Kettara intrusion and deposit are weakly metamorphosed pelites with thin-bedded sandstone and local sandstone and limestone layers (Sarhlef schists; Huvelin, 1977), which are crosscut by numerous mafic and felsic dykes belonging to the bimodal magmatic association. Geochemical data for the Sarhlef schists indicate that they are likely to be derived from an active continental margin (Moreno et al., 2008; Essaifi et al., 2014). Around the Kettara massive sulfide deposit, these host rocks are cut by numerous quartz and quartz-calcite veins, some of which are sulfide-bearing. Due to the limited availability of underground samples at Kettara, this research focuses on these veins to understand the fluids that circulated around the massive sulfide deposit. 60 rock samples including host rocks, mineralized veins and ore samples were collected from outcrops, ore stockpiles present in the mine site and drill core from the Kettara deposit.

3. Deformation and hydrothermal alteration

3.1. Structure

The Kettara region exemplifies the style of deformation in the central Jebilet. The Kettara deposit and intrusion are located within the network of anastomosing ductile shear zones that characterize the central Jebilet block (Essaifi et al., 2001) (Fig. 2A). They are located to the south of the Mesret Fault termination, marked by a number of SE-trending synthetic dextral faults showing a horsetail pattern (Fig. 1C and Fig. 2A). To the south-west of Kettara lies the Oled Har intrusion and to the northeast the Safsafat intrusions, together these form a N-S magmatic lineament which is curved in the Kettara area (Fig. 2A). The Oled Har and Safsafat intrusions are emplaced along N-S sinistral shear zones (Fig. 2B). The Kettara intrusion and deposit are located in a step-over zone between the end of the N-S strike-slip Oled Har shear zone and the beginning of the N-S strike-slip Safsafat shear zone (Fig. 2B).

Within the Kettara sector, the structures observed include both ductile structures related to the main Variscan shortening and brittle structures related to later stages of the Variscan deformation (Fig. 2B). The post-Visean main Variscan shortening has caused regional folding as well as a progressive transposition of the original bedding (S_0) into a single and penetrative sub-vertical chlorite-muscovite bearing schistosity (S_1), contemporaneous with a low-grade greenschist facies regional metamorphism. This regional schistosity is axial planar to upright, moderately to gently (60–20°) NE-plunging folds (Fig. 3), and bears a gently plunging stretching lineation, which becomes down-dip near the intrusion (Fig. 3; Essaifi et al., 2001). In plan view, schistosity trajectories in the Kettara area display progressive curvatures from the NNE–SSW regional direction towards ENE–WSW directions indicating dextral shearing (Fig. 2B, C). Strain gradients accompany the curvatures of the S_1 cleavage trajectories. The zones of most intense shearing are marked by very intense S_1 schistosity, thinning of original beds, and isoclinal folding (Fig. 3). In the host schists located between the deposit and the intrusion (Fig. 4A), bedding is transposed into the penetrative S_1 schistosity, which is characterized by a strong S-fabric of quartz grains and by well-developed pressure shadows around oxide minerals (ilmenite, anatase and hematite; Fig. 5A, B). Kink bands and micro-scale S/C shear bands (Berthé et al., 1979) are well developed in the zones of most intense shearing where phyllites are intensively stretched along S and C planes. The host sandstone layers are progressively boudinaged and transposed into the S_1 cleavage. Numerous sigmoidal quartz veins cross-cutting the schistosity at low angles are observed in the wall rocks adjacent to the deposit (Fig. 3 and Fig. 4B). On the northern side of the deposit (the hanging wall), deformation decreases progressively northwards. Thin calcareous beds intercalated within the metapelites are increasingly thinned as the gossan is approached, varying from centimeter- to meter-scale lenses of fine-grained bioclastic limestone and calcareous sandstone proximal to the deposit, to a coarse-grained layered calcareous sandstone bed that forms a stratigraphic horizon located 1.5 km from the deposit (Fig. 2C).

In the Kettara intrusion, deformation is very heterogeneous. Meter to centimeter-scale anastomosing shear zones bound lenticular meter to 100 m-scale domains of weakly deformed to undeformed gabbros (Fig. 2C and Fig. 3). Numerous subvertical felsic and mafic dykes cut across the intrusion and the host rocks. Mafic dykes up to 10 m wide cross-cut the schistosity in the vicinity of the Kettara deposit, but are locally deformed at their margins and boudinaged into lenses. One dyke appears to be cross-cut by the gossan of the Kettara deposit; and Huvelin (1977) describes meter-scale lenses of dolerite within the massive orebody, suggesting that the dyke pre-dated the sulfide deposit.

To summarize, we interpret that the Kettara area is located between two adjoining *en échelon* shear zones and has been deformed in order to accommodate continued strike-slip displacement. In this model, a short ENE-WSW trending dextral shear zone connects the terminations of 2 N-S striking *en échelon* shear zones. In agreement with sinistral shear sense criteria inferred from schisotosity trajectories, and attested by multiscale S/C shear bands and various microscale shear criteria as rotation of contact metamorphism porphyroblasts or asymmetric pressure shadows along the Oled Har and Safsafat *en echelon* shear zone segments (Essaifi, 1995), the Kettara step-over zone is inferred to have acted as a compressional 'jog' or a 'push-up' area.

3.2. Hydrothermal alteration in the Kettara intrusion

The structural relationships between the intrusion and the host rocks show that the Kettara intrusion was emplaced in a zone of regional dextral shearing (Ait Tahar, 1987; Essaifi 1995). Two periods of deformation and subsequent hydrothermal alteration have been distinguished within the intrusion (Essaifi et al., 2004). The first of these occurred during cooling of the intrusion, with formation of cm-scale shear zones. Introduction of fluids rich in Si, Ca and Mg, pervasive throughout the intrusion, led to the formation of amphibole-rich ultramylonites from original gabbros (Essaifi et al., 2004). The second episode followed the thermal re-equilibration of the intrusion. Fluid flow was focused along the shear zones with retrogression to chlorite and leaching of Na, Si, Ca and Mg (Essaifi et al., 2004).

Two types of mesocopic veins are associated with shear zones in the Kettara intrusion (Essaifi et al., 2004): (a) quartz-chlorite veins up to 10 cm wide at the center of the chlorite-rich shear zones, and (b) up to 30 cm wide quartz-calcite '*en echelon*' or sigmoidal veins (Fig. 4D), with quartz at the vein boundaries and calcite along the center of the veins. These veins strike at 45° relative to the direction of the shear zones in low strain areas, but they are progressively reoriented and deformed in the vicinity of those shear zones (Essaifi et al., 1995). Such geometric relationships indicate that formation of quartz-calcite veins was contemporaneous with shear zone development.

The quartz veins are stretched parallel to shear zones and show evidence of recrystallization of quartz grains. According to the geometric relationships between the veins and the shear zones, the quartz veins in the inner parts of the shear zones are considered to be the earliest ones and served as nucleation sites for the shear zones (Segall and Simpson 1986), whereas those oblique to the foliation (the quartz-calcite veins) were emplaced slightly later during widening of the shear zones (Gates and Speer, 1991). Thus the quartz-chlorite veins would be relatively earlier than those filled by quartz-calcite (Fig. 3), indicating the fluid evolution within the Kettara intrusion.

3.3. Hydrothermal alteration in the host rocks

In the Kettara area, the schists are devoid of any volcanic units and are dominantly composed of light grey pelites (black shales) intercalated with thin beds of fine-grained sandstone and limestone, with a well-developed schistosity. The pelites are dominated by a muscovite-quartz-chlorite-albite mineral assemblage (Fig. 5A), with muscovite grains showing pressure shadows and an oblique orientation to S_1. In the sandstone layers, mineralogy is dominated by quartz and feldspar with quartz having an average grain size of 50 μm and forming up to 95 vol. % of the rock.

Approaching the intrusion boundaries, a low pressure/high temperature syntectonic contact metamorphism assemblage is developed: chlorite crystals increase in size while crystals of biotite appear along the cleavage plane. About 15m from the contact with the leucogabbros, contact metamorphic minerals (andalusite or cordierite) are developed. They form elliptical spots flattened and stretched along the cleavage plane. Hydrothermal alteration in the contact metamorphic aureole is very intense. It is marked by retrogression of the contact metamorphic minerals into secondary minerals. Biotite grains in the matrix are chloritized; cordierite and andalusite porphyroblasts are completely altered to chlorite, muscovite and quartz.

Approaching the Kettara gossan, the pelites become greenish then purple in the gossan. At the margin of the deposit muscovite is aligned along the schistosity plane (S_1); Fe-rich chlorite appears at a distance of 10 m from the gossan and its abundance increases towards the gossan in both footwall and the hanging wall. Sericite is locally oblique to the foliation plane, and its content increases towards the gossan, especially in the hanging wall of the deposit. The adjacent areas of the gossan are also characterized by the occurrence of numerous centimeter-scale quartz ± calcite mineralized veins. These mineralized veins have gradational to sharp boundaries and cut the schistosity in the host rocks (Fig. 3 and Fig. 4B), but are affected by kink bands and also carry a recrystallized quartz fabric, indicating their syn-tectonic nature. The veins have the same mineralogy as the massive pyrrhotite ore body, being composed of a quartz-chlorite gangue enclosing grains of pyrrhotite, chalcopyrite, sphalerite, arsenopyrite, galena, and native bismuth. Phosphate minerals and zircon are also found in the mineralized veins. In some veins the sulfide minerals develop in layers that are in continuity with the pelite layers of the host schists. They occur between the quartz grains or in association with chlorite in the vein margins. Thus the pelite banding persists through the veins by alternation of sandstone layers composed of fine-grained quartz (0.1 mm) and layers composed of coarse-grained quartz associated with chlorite and sulfides which have replaced former pelite layers. The structural relationships indicate that these veins were emplaced towards the end of the ductile deformation phase. These quartz-chlorite-pyrrhotite-bearing veins are crosscut by carbonate and pyrite-bearing veins (Fig. 4F). The massive pyrrhotite is cross cut by carbonate veins (Fig. 4E). However quartz-chlorite veins cutting across massive pyrrhotite have never been observed. The field relationships now observed indicate that the chlorite-schists developed around the Kettara deposit result from syntectonic hydrothermal alteration of the host rocks. According to Bernard et al. (1988), this metasomatic alteration was accompanied by leaching of Si and Ca that subsequently crystallized as quartz-calcite veins within the wall rocks of the orebody.

3.4. The Kettara massive sulfide deposit

The core of the Kettara deposit is a massive sulfide lens dominated by pyrrhotite, but with gradational margins. These margins are clear in core from inclined borehole K101, which extends to a depth of 193 m through the Kettara deposit, intersects the central part of the ore body at depths of 159–179 m, and shows the contact between the sulfide lens and the pelitic host rocks. The margins of the mineralized horizon contain numerous fragments of foliated wall rocks surrounded by irregular veins of pyrrhotite, and aligned parallel to the foliation (Fig. 4E). Pyrrhotite has crystallized parallel to the main schistosity and also fills fractures that cut across the foliation in the host rocks at the boundaries of the ore body (Fig. 4E). Moving inwards from the margin, the wall-rock fragments become smaller and less abundant. Away from the margins, the core of the deposit is dominated by massive pyrrhotite including only patches of the host rocks (Fig. 5C).

Study of mineralized samples, from core and from the stockpile, has allowed characterization of the primary mineralization of the Kettara deposit. The main mineralization is represented by fine-grained massive to semi-massive pyrrhotite. It is composed of pyrrhotite (70-90%), chalcopyrite (5-25%), magnetite (3-5%), sphalerite (2%), arsenopyrite (<1%) and traces of galena and native bismuth (Fig. 5D). The gangue minerals are quartz and chlorite, which can be associated with talc and mica, or enclose phosphate minerals and Ti-oxides. The semi-massive ore is characterized by a chlorite-rich gangue and pyrrhotite oriented parallel to the main schistosity (Fig. 5C).

Pyritic ore occurs as cm-scale veins or pods cutting the semi-massive to massive pyrrhotite, the pyrrhotite mineralized veins and the host schists (Fig. 5E, F). It is composed of centimeter-scale brecciated pyrite cubes together with rare marcasite and chalcopyrite associated with a gangue of carbonates. The pyritic ore has been affected by deformation within brittle to semi-brittle shear zones (Brown and McClay, 1993) but is clearly unaffected by ductile deformation. Pyrite crystals are locally fractured and brecciated (Fig. 5F), but lack features associated with ductile deformation such as pressure shadows. These microstructural relationships indicate that the pyritic ore post-dates the main period of ductile deformation (Marshall and Gilligan, 1993). Euhedral crystals of pyrite are also disseminated in the hanging wall of the ore lens.

Field and textural relationships show that two successive mineralizing fluids contributed to the formation of the Kettara deposit (Fig. 6): (i) the first fluid led to formation of a pyrrhotite-chalcopyrite-sphalerite-magnetite-arsenopyrite paragenesis and a quartz-chlorite gangue. This mineralogical association is affected by ductile shearing, marked by orientation of pyrrhotite and chalcopyrite along the schistosity and shearing planes; and (ii) the second fluid led to deposition of pyrite and carbonates, which are affected by brittle cataclasis.

Chlorite, the main alteration product in the shear zones of the Kettara intrusion, is also the main gangue mineral in the Kettara massive sulfide deposit. Chlorites associated with the mineralization are Fe-rich (0.5≤ XFe ≤ 0.85, Souaré 1988), in common with the shear zones inside the intrusion (0.46 ≤ XFe ≤ 0.48, Essaifi et al., 1995). This similarity in chlorite composition was the first suggestion that the same fluid led to the formation of the massive sulfide and the chlorite schists of the Kettara intrusion (Essaifi et al., 1995; Essaifi and Hibti, 2008).

It is clear from the field relationships that there was significant hydrothermal fluid flow in the Kettara area associated with the Variscan deformation, and with the syn-tectonic intrusions in the area. This has led to hydrothermal alteration and veining around both the Kettara intrusion and the deposit. However, it is not evident from field relationships alone whether the Kettara sulfide deposit was formed prior to this deformation period, with its own hydrothermal aureole, and was then subsequently deformed; or whether it formed at the time of intense late-tectonic hydrothermal activity. In order to investigate this question, we have studied fluid inclusions and isotopic compositions in the hydrothermally altered rocks of Kettara.

4. Sampling and analytical techniques

Fluid inclusions were analyzed in order to characterize the composition of the hydrothermal fluids and to estimate their entrapment conditions. Five samples were studied, two from the mineralized veins adjacent to the Kettara deposit and three from the mafic-ultramafic intrusion. Microthermometric fluid inclusions study was performed at Cadi Ayyad university using a Chaixmeca microthermometry apparatus (Poty et al. 1976), calibrated by standard synthetic fluid inclusions: i/ H_2O-CO_2 inclusions with the melting of solid CO_2 at −56.7 °C, ii/ pure H_2O inclusions (ice melting at 0.0 °C), and iii/H_2O-NaCl with eutectic temperature at −21.2 °C. These data have been verified at Lille 1 University where additional microthermometric data were obtained using a FLUID INC (USGS-type) heating and freezing stage, calibrated by standard synthetic fluid inclusions: i/ H2O-CO_2 inclusions with the melting of solid CO_2 at -56.6 °C, ii/ pure H_2O inclusions (ice melting at 0.0 °C) and iii/ homogenization temperature of pure H_2O inclusions at 374.1 °C. The precision of measurement is ±0.1 and ±0.5 at low- and high-temperature respectively. Semi-quantitative compositional data of inclusion gases were calculated from Laser Raman spectra at Lille 1 University. The Raman spectra were measured using a LabRam HR800 Jobin-Yvon_ microspectrometer equipped with 1800 g/mm gratings and using 532.28 nm (green) laser excitation. Acquisition time span varied from 20 to 60 s during three accumulating cycles. The spectra regions scanned were in the range 1000-1500 cm-1 for CO_2, 2250–2750 cm^{-1} for N_2 and H_2S and 2750–2950 cm-1 for CH_4.

O/H isotope analyses were conducted on quartz and chlorite separated from the intrusion, the deposit, and the mineralized vein adjacent to the deposit. Measurements of oxygen isotope compositions were performed at the stable isotope laboratory of the University of Lausanne following the procedures described by Lacroix and Vennemann (2015). Oxygen isotope compositions are given in the standard δ-notation, expressed relative to VSMOW in permil (‰), and the average precision is ±0.1‰.Measurements of hydrogen isotope compositions of chlorite were performed at the University of Lausanne following the procedures described by Leclère et al. (2014). The results are given in the standard δ-notation, expressed relatively to VSMOW in permil (‰), and the precision is better than ± 2‰.

5. Stable isotopes

Chlorite and quartz from both the Kettara deposit and the intrusion have been studied for their oxygen and hydrogen isotope compositions. Hand-picked chlorite crystals from samples of the massive pyrrhotite ore yield $\delta^{18}O$ and δD values of 6.24‰ (VSMOW) and -48‰

(VSMOW), respectively (Table 1). Chlorite separated from the pyrrhotite bearing mineralized-veins yield respectively $\delta^{18}O$ and δD values of 7.8‰ (VSMOW) and -52‰. Chlorite separated from the quartz-chlorite veins associated with the shear zones in the intrusion has $\delta^{18}O$=4.4‰ and δD=-52‰. Chlorite separated from the chlorite schists in shear zones within the Kettara intrusion has $\delta^{18}O$=6.01‰ (Essaifi et al., 2004). The oxygen isotopic composition of chlorite from the Kettara deposit is thus very similar to that from the mineralized veins in its wall rocks and to the chlorite-rich shear zones cross-cutting the Kettara intrusion, supporting the hypothesis that alteration in the deposit, its wall rocks and the intrusion could be related to the same hydrothermal activity.

Hand-picked quartz crystals from the mineralized veins at the margins of the Kettara deposit yield $\delta^{18}O$ values of 9.1‰, and quartz from the veins associated with the shear zones in the Kettara intrusion yields $\delta^{18}O$ values of 9.8‰ (Table 1). The similarity between the $\delta^{18}O$ isotopic compositions of quartz from the mineralized veins in the wall rocks of the Kettara deposit and from quartz-chlorite veins associated with the shear zones within the intrusion indicates that formation of both the mineralized and un-mineralized veins could be related to the same fluids.

Composition of the hydrothermal fluid in the intrusion and the deposit has been calculated using the oxygen fractionation between chlorite and water determined by Cole and Ripley (1998) and Zheng (1993), at temperatures corresponding to the upper greenschist facies (300–400°C). The results give similar values of the hydrothermal fluid, for both calibration curves, between 6.0 and 7.2 ‰ (VSMOW). Such fluid compositions could either correspond to magmatic water or metamorphic water (Sheppard, 1986) (Fig. 7). For hydrogen, the chlorite-water calibration of Taylor (1974)was chosen. The δD values of the fluid are calculated to be between −14.5‰ and −10.5 (VSMOW), which corresponds more clearly to metamorphic water (Fig. 7).

6. Fluid inclusions

Fluid inclusion studies have been studied in both the quartz-bearing unmineralized veins of the Kettara intrusion and the mineralized veins adjacent to the sulfide deposit. The descriptions below are based on criteria proposed by several authors to classify and determine the origin and content of fluid inclusions (e.g., Bodnar, 2003; Van Kerkhof and Hein, 2001). The vapor-filling ratio (R_{flv}) has been estimated at the ambient temperature based on Shepherd's chart (Shepherd et al., 1985).

In the Kettara intrusion fluid inclusion studies were conducted on quartz and calcite from two quartz−chlorite veins ($V_{q\text{-}cl}$) and one quartz-calcite vein ($V_{q\text{-}cc}$). According to the phase number at room temperature, many fluid inclusion types have been identified. Microthermometric analysis and Raman spectrometry allowed classification of these inclusions into five types (Table 2): type 1 = H_2O-CO_2-Salt, type 2 = CO_2-N_2-CH_4, type 3 = H_2O-(Salt), type 4 = H_2O-N_2-CH_4 and type 5 = H_2O. Type 2 inclusions exist in both the quartz-chlorite and the quartz-calcite veins. The quartz-chlorite veins ($V_{q\text{-}cl}$) contain also type 1 and type 3 inclusions whereas the quartz-calcite vein ($V_{q\text{-}cc}$) contains type 4 and type 5 inclusions (Fig. 8 and Fig. 9).

Type 1 inclusions are dominantly three-phase inclusions (2 liquids and a vapor, L1+L2+V). They coexist with two-phase inclusions with a thick vapor meniscus and numerous multiphase inclusions containing a solid phase (L1+L2+V+S). Their size varies from 10 to 40 µm and R_{flv} from 5 to 10%. The melting temperatures of carbon dioxide (T_{mCO2}) are distributed between −61.1 and −56.7°C with a mean value at −58.5 °C, which are close to the $TmCO_2$ of pure CO_2 (−56,6 °C) (Fig. 10A). Clathrate melting temperatures $T_{m(cl)}$ are overall between −9.6 and 10.5 °C. The lower values of $T_{m(cl)}$ were recorded by three-phase (L1+L2+V) inclusions (≈−8 °C) whereas the higher $T_{m(cl)}$ were collected in multiphase

(L1+L2+V+S) inclusions (≈ 9.2 °C). Homogenization of CO_2 occurs either in the liquid phase, with $T_{h(CO2)(L)}$ *ranging* from 24.6 to 29.9 °C, or the vapor phase, with $T_{h(CO2)(V)}$ ranging from 26.3 to 28.7 °C (Fig. 10B). Ice melting temperature $T_{m(ice)}$ values are between −25.3 and −22.7 °C (mean = −24.1 °C) (Fig. 10C). Bulk homogenization temperature (T_h) occurs either into liquid ($T_{h(L))}$ or critical phase $T_{h(c).}$ $T_{h(L)}$ is between 300 and 366 °C, $T_{h(c)}$ ranges from 321 to 409 °C. Decrepitation occurs sometimes before bulk homogenization and decrepitation temperatures (T_d) are between 326 and 416 °C (Fig. 10D).

Type 2 inclusions are one-phase inclusions encountered in the quartz-chlorite veins ($V_{q\text{-}cl}$) and the quartz-calcite vein ($V_{q\text{-}cc}$) as well. These inclusions are less abundant and are often associated with type 1 inclusions. In $V_{q\text{-}cl}$, T_{mCO2} occur between −58.3 and −57.1 °C and homogenization occurs in the liquid phase with T_{hCO2} ranging from 11.2 to 26.2 °C (Fig. 10E, F). The inclusions are composed of CO_2, N_2 and CH_4. According to the semi-quantitative composition (X in mole percent) of gases calculated from Raman spectrum areas, XCO_2 varies from 84.6 to 97.9 mol %, XN_2 from 0.4 to 9.6 mol % and XCH_4 from 0 to 5.9 mol %. In $V_{q\text{-}cc}$, type 2 inclusions exist either as primary inclusions with a dark appearance or as secondary inclusions in transgranular plans. The secondary inclusions have a bright appearance and coexist with FIA of type 3. $T_{m(CO2)}$ and $T_{h(CO2)}$ of primary inclusions are −58.7 and −14.0 °C respectively and the values collected on one secondary inclusion are −57.4 and 5.7 °C respectively (Fig. 10E, F). The average proportion of gases in primary inclusions is XCO_2 = 59 mol %, XN_2 = 35 mol % and XCH_4 is about 6 mol %, and for secondary inclusion XCO_2 = 78 mol %, XN_2 = 19 mol %, XCH4= 3 mol %.

Type 3 inclusions are two-phase at room temperature and are present in the quartz-chlorite veins ($V_{q\text{-}cl}$). They are composed of two-phase inclusions sometimes presenting a solid phase. These fluid inclusions occur as primary and as secondary inclusions. The primary inclusions have a size of 5 to 15 µm. They have an irregular shape with often a very thin tip elongated in the crystal. The largest inclusions are commonly shredded. Their average vapor-filling ratio (R_{flv}) is around 10%, but can reach 20% when the solid phase is missing. $T_{m(ice)}$ are between −24.3 and −17.0 °C with a mean value of −22.2 °C (Fig. 11A). Considering the small size of this fluid inclusion population, we could observe only one solid melting at a temperature (T_s) of 278.2 °C. $T_{h(L)}$ range from 149 to 261 °C with a mean value at 216 °C (Fig. 11B). Secondary inclusions have a small size (about 5 µm). Their average $T_{m(ice)}$ is around −21.8 °C and their $T_{h(L)}$ range from 135 to 169 °C with a mean value of 156 °C (Fig. 11A, B). Using either $T_{m\ (ice)}$ or T_s, calculated salinities of primary fluid inclusions are 23.8 and 36.7 wt. % NaCl respectively (Bodnar and Vityk, 1994).

Type 4 inclusions consist of two-phase (L, V) fluid inclusions located in growth zones of quartz crystals of the quartz-calcite veins ($V_{q\text{-}cc}$). The inclusions are generally shredded or have irregular shapes. They are essentially two-phase inclusions with a dark appearance, R_{flv} from 5 to 30 % and a mean size of 10 µm. $T_{m(ice)}$ values are between −4.0 and −0.5 °C with a mean value of −1.9 °C in $V_{q\text{-}cc}$(Fig. 11C). $T_{h(L)}$ range from 205 to 255 °C with a mean value of 240 °C (Fig. 11D). The vapor phase is mostly composed of nitrogen and methane with average mol fractions at 86.1 and 13.9 mol% respectively.

Type 5 inclusions occur in $V_{q\text{-}cc}$ where they have a pseudo secondary or secondary origin in quartz and a primary origin in calcite. In quartz they are located in microcracks showing intragranular grain boundaries-grain internal or transgranular trails according to descriptions of Van den Kerkhof and Hein (2001). Their average size is about 5 µm with a constant R_{flv} in all inclusions (≈5%). In calcite, they are generally elongated concurrently with the calcite growth direction. Their R_{fl} are about 5% and their size range from 4 to 15 µm. The mean value of $T_{m(ice)}$ is −0.1 °C in the quartz and around −1.5 °C in calcite (Fig. 11C). The average $T_{h(L)}$ is 180 °C in quartz, while in calcite $T_{h(L)}$ are a bit lower and range from 131 to 187 °C with a mean value of 156 °C (Fig. 11D). The corresponding salinities are relatively low, 0.2 wt. % NaCl in quartz and around 2.6 wt. % NaCl in calcite (Bodnar and Vityk, 1994).

In the mineralized veins adjacent adjacent to *the Kettara deposit* fluid inclusions were studied in quartz associated with pyrrhotite mineralization from a quartz mineralized vein crosscut by carbonates ($V_{m\text{-}qc}$) and a quartz-chlorite mineralized vein ($V_{m\text{-}qcl}$). Carbonates associated with pyrite mineralization were not suitable for fluid inclusion studies because they are less transparent and poor in fluid inclusions. Based on petrographic observations, microthermometric analysis and Raman microspectrometry, different fluid inclusion types have been distinguished and are summarized in table 2.

According to petrographic observation, fluid inclusions in the two mineralized veins consist mainly of two phase and one-phase fluid inclusions at room temperature and scarce inclusions containing a solid phase. After microthermometric and Raman spectrometry analyses, six fluid inclusion types have been identified, not all present in the same sample. Type 1 consists of H_2O-CO_2-N_2-CH_4 fluid inclusions; type 2 inclusions are composed of CH_4-N_2-CO_2; type 3 of H_2O-salt, type 4 of H_2O-CH_4; type 5 of N_2-CH_4 and type 6 of CH_4 (Fig. 12). The type 3 inclusions exist in both the quartz-chlorite and the quartz mineralized vein crosscut by carbonates. The quartz mineralized vein crosscut by carbonates ($V_{m\text{-}qc}$) contains also types 1 and 2 whereas the quartz-chlorite mineralized vein ($V_{m\text{-}qcl}$) contains types 4, 5 and 6.

Type 1 inclusions are two-phase at room temperature with R_{flv} between 5 and 10%. Their size varies from 5 to 50 µm (mean of 20 µm). The inclusions have a rounded or rectangular elongated shape. In these inclusions $T_{m(ice)}$ ranges from −9.1 to 0.0 °C with a mean value of −3.6 °C (Fig. 13A), T_h is between 178 and 230 °C with an average of 210 °C (Fig. 13B), and $T_{m(cl)}$ ranges from 2.9 to 10.1 °C with a mean value of 6.2 °C. The vapor phase of these inclusions is composed of variable proportions of carbon dioxide, nitrogen and methane. CO_2 and CH_4 are present in all inclusions whereas nitrogen is often missing or its content is lower than the detection limit. X_{CO2} varies from 8.7 to 84.1 mol %, X_{CH4} varies from 8.4 to 51.5 mol %, and when nitrogen, is detected X_{N2} ranges from 17.9 to 79.0 mol %. Their average composition is 44.0mol % CO_2, 21.7mol % CH_4 and 34.4 mol %N_2.

Type 2 inclusions are one phase at room temperature and are commonly observed in the same fluid inclusion assemblages (FIA, Goldstein and Reynolds 1994) than type 1. They are less abundant and have a dark appearance with often an exceptional large size of 60 µm. No visible aqueous phase was detected during microthermometric experiments. Only T_h has been measured in these inclusions. It occurs either into liquid or vapor phase, with values of $T_{h(L)}$ ranging from −99.4 to −70.4 °C (mean = −91.4 °C) and $T_{h(V)}$ from −95.9 to −78.3 °C (mean = −88.9 °C). Raman analysis shows that they are composed of CO_2 (from 11.5 to 27.0 mol %), N_2 (from 21.0 to 38.1 mol %) and CH_4 (from 36.1 to 67.5 mol %). The mean values of these gas show the predominance of methane (X_{CH4} = 48.0 mol %) followed by nitrogen (X_{N2}= 31.9 mol %) and then by carbon dioxide (X_{CO2} = 20.0 mol %).

Type 3 inclusions exist in both the quartz mineralized vein crosscut by carbonates ($V_{m\text{-}qc}$) and in the quartz-chlorite mineralized vein ($V_{m\text{-}qcl}$).They have a bright aspect and contain two phases at room temperature. In $V_{m\text{-}qc}$ their size is generally about 5 to 30 µm with relatively large R_{flv} (5 to 20%). In $V_{m\text{-}qcl}$ they have an irregular shape with sometimes a thin tip oriented in the crystal growth direction which could indicate a primary origin of these inclusions. Their R_{flv} range from 5 to 10% and the $T_{m(ice)}$ are between −7.9 and −2.0 °C in $V_{m\text{-}qc}$ and between −17.4 and −0.6 °C in $V_{m\text{-}qcl}$, with mean values of −4.7 and −6.3 °C respectively (Fig. 13D). Their T_h range from 176 to 258 °C (mean = 224 °C) for $V_{m\text{-}qc}$ and from 174 to 260 °C (mean = 218 °C) for $V_{m\text{-}qcl}$ (Fig. 13F). So, in $V_{m\text{-}qc}$ salinities are between 3.4 and 11.6 wt.% NaCl and in $V_{m\text{-}qcl}$ they range from 1.1 to 20.5 wt.% NaCl. According to the frequency plot of $T_{m(ice)}$ (Fig. 13E), the maximal frequency of $T_{m(ice)}$ corresponds to the mean value in $V_{m\text{-}qc}$ (−4.7 °C), whereas in $V_{m\text{-}qcl}$ the value of maximal frequency is a bit lower than the mean value and is around −5.0 °C. The salinities from these values are 6.9 and 7.9 wt. % NaCl respectively.

Type 4 inclusions are two phase fluid inclusions showing a regular shape. They appear dark and are particularly abundant in quartz wrapped by sulfides. Their average size is about 10 µm with an R_{flv} around 5 and 20 %. One inclusion of this group contains exceptionally a solid phase, which is considered as accidental solid due to the lack of other solid phases in the surrounding inclusions. $T_{m(ice)}$ range from −19.2 to −0.3 °C with a mean value of −6.0 °C (Fig. 13A). T_h range from 212 up to 376 °C with a mean value around 290°C (Fig. 13B), and the mean value of $T_{m(cl)}$) is around 8.6 °C. The Raman analysis indicates that the vapor phase is composed exclusively of methane and the accidental solid is graphite.

Type 5 inclusions are represented by dark monophase fluid inclusions and form sometimes FIA with type 4 inclusion. They are more abundant in some quartz crystals and have a sub-regular shape. During cooling runs these inclusions showed only a $T_{h(V)}$ ranging from −124.1 to −105.2 °C with a mean value of −120 °C, and one $T_{h(L)}$ observed at −121.1 °C (Fig. 13C). The Raman analysis indicates the presence of nitrogen and methane with X_{N2} varying between 49.8 and 60.4 mol % and X_{CH4} between 39.6 and 50.2 mol %.

Type 6 inclusions consist of monophase secondary fluid inclusions located along transgranular trails with inclusion sizes reaching 40 µm. As in type 4 inclusions, one inclusion of this group contains an accidental solid. Their microthermometric data are: $T_{h(CH4)(L)}$ between −97.4 and −93.4 °C and $T_{h(CH4)(V)}$ between −85.5 and −82.0 °C (Fig. 13D). The higher limit (−82.0 °C) is almost equal to the critical temperature of methane ($T_{critical}$ = −82.1 °C, Ruano 2008). The Raman analysis indicates that these inclusions are filled only by CH_4 and that the accidental solid is graphite.

7. Discussion

7. 1. Sources of fluid inclusions

The microthermometric study and Raman analysis showed a wide variety of fluid inclusion types in the mineralized veins adjacent to the massive sulfide ore and the unmineralized veins in the mafic-ultramafic intrusion, but also at the sample scale. The main systems encountered in the veins can be grouped into H_2O-(CO_2,-N_2-CH_4) ±Salt, CO_2-N_2-CH_4, H_2O-(Salt), H_2O-CH_4±Salt, H_2O-CO_2-Salt, N_2-CH_4 and CH_4 systems. They belong to three main fluid types: 1/ a H_2O-salt fluid with extremely variable salinities, from pure water to quasi-saturated brines; 2/ a volatile-rich (CH_4-N_2-CO_2) fluid with variable proportions of each component ranging from pure component (pure CH_4), binary mixtures (CH_4-N_2) to ternary mixtures (CO_2-CH_4-N_2); 3/ a mixed H_2O-salt-volatiles fluid; note that H_2S was never found. These fluids can be linked to three distinct sources (Sheppard, 1986): (i) metamorphic fluids (H_2O-CO_2-CH_4-N_2); (ii) magmatic fluids (H_2O - salt (Na, K, Li)); and (iii) basinal fluids (H_2O-hydrocarbon-salt). According to Thiéry et al. (1994), the ternary CO_2-CH_4-N_2 system is common in fluid inclusions representative of diagenetic, hydrothermal and metamorphic fluids.

CH_4 or a mixture of CH_4 and N_2 always dominates the volatiles in the mineralized veins, whereas CO_2 occurs in minor proportions or is absent. In contrastCO_2 is always the dominant species relative to CH_4 and N_2 in the unmineralized veins associated with the shear zones within the intrusion (Fig. 14). CH_4 and CH_4-N_2 indicate reducing conditions, which seem to characterize the mineralized veins adjacent to the deposit.

The variability of compositions, homogenization temperatures and salinities may be attributed to three main phenomena: cooling, boiling or fluid mixing in addition to post-trapping processes. The graphical representation of T_h versus $T_{m(ice)}$ of fluid inclusions containing an aqueous phase allows us to identify the major trends of these mechanisms (Fig. 15).

In the mineralized veins adjacent to the Kettara deposit, the co-existence in the quartz mineralized vein crosscut by carbonates (V_{m-qc}), of water+volatile (H_2O-CO_2-N_2-CH_4, type 1) and volatile-rich (CH_4-N_2-CO_2, type 2) inclusions in the same FIA is probably an indication of boiling or mixing. This hypothesis is corroborated by the slight evolution of $T_{m(ice)}$ relative to T_h, (Fig. 15A). In addition, the composition of the vapor phase (CH_4-N_2-CO_2) of type 1 inclusions is similar to type 2. Final homogenization temperatures of type 1 and type 3 inclusions are almost identical (210–220 °C respectively), which also supports a boiling process by which the separation of volatile phases from the liquid phase occurred, causing the salt concentration in the residual liquid. Fluid inclusions resulting by this process give a similar T_h range. Accordingly the T_h of both types (210–220°C) can be considered as the minimal trapping temperature of the inclusions.

In the quartz-chlorite mineralized vein ($V_{m\text{-}qcl}$), there is a linear distribution of type 3 and type 4 fluid inclusions along the T_h axis indicating a more significant variation of T_h than salinities. This distribution mode is characteristic of cooling for both fluid inclusion types (Fig. 15B). On the other side, we also observe that relatively high T_h are recorded by type 4 fluid inclusions (up to 370 ° C) compared to type 3 (< 270 °C). This highest T_h suggests the trapping of two immiscible phases in type 4 inclusions (H_2O-CH_4) and indicates a mixing process probably between those of type 3 (H_2O) and type 5 (N_2-CH_4). After Holloway (1984), the immiscibility between CH_4 and H_2O could result in the common occurrence of methane as natural gas in low-grade metamorphic terranes. Otherwise, the absence of N_2 in type 4 inclusions remains unexplained.

In the Kettara intrusion, the distribution of fluid inclusion data in quartz-chlorite veins (V_{qcl}) shows a decrease of T_h at nearly constant salinity, in favor of a cooling in the system. This is valid for primary type 3 ($T_{m(ice)}$ = −22.2 °C, Th = 220 °C), but also for secondary type 3 fluid inclusions ($T_{m(ice)}$= −21.8 °C, Th = 160 °C) (Fig. 15C). Type 1 inclusions belong to the general system H_2O-CO_2-salt. Their relatively high $T_{h(L)}$= 350 °C, their homogenization in the critical phases and their high salinity evident from their low $T_{m(ice)}$(−24.1 °C) can be explained by the trapping of a fluid in an immiscible state, probably resulting from mixture between a magmatic fluid represented by type 3 (H_2O-salt) inclusions and a metamorphic fluid represented by type 2 (CO_2-N_2-CH_4) inclusions. A mixing processes can therefore explain the presence of the type 1 and types 2 inclusions in the same FIA. Whilst boiling is not ruled out, the absence of water in the type 2 inclusions is incompatible with phase separations during this process (e.g., Lawrence et al., 2013), unless the water meniscus is not visible.

In the quartz-calcite vein, the relationship between inclusions containing an aqueous phase is difficult to establish because they do not belong to the same generation and do not have the same compositions (Type 3, 4 and 5). The presence of type 4 (H_2O-N_2-CH_4) and type 2 (CO_2-N_2-CH_4) inclusions in quartz lead us to consider a boiling process. This would explain the absence of CO_2 in type 4 inclusions. However, it does not explain the apparent absence of water in type 2 inclusions although the most recently formed are generally close to aqueous bearing inclusions (Fig. 8). However, a small amount of invisible water can be present along the rims of these fluid inclusions (Roedder, 1984).

The types of volatile phases and the salinities of the fluid inclusions are compatible with a model involving mixing of metamorphic H_2O - (CO_2, N_2, CH_4) and magmatic (H_2O-Salt) fluids in the Kettara shear zones. This is consistent with the stable isotope data, which also indicate a metamorphic origin for the hydrothermal fluids. The Kettara shear zones represent pathways for upwardly directed and focused fluid flow, and their interconnection allowed fluid flow to be channeled at the regional-scale (Essaifi et al., 2004). However, a key question is how this fluid flow relates to the formation of the Kettara massive sulfide deposit.

7.2. Microstructural timing of mineralization

It is clear that the Kettara pyrrhotite massive ore has been affected by the ductile Variscan deformation. However, the overall relationships are potentially compatible with either: i) remobilization of a pre-tectonic, syngenetic ore body; or ii) syn-deformational, epigenetic emplacement of the ore body (Marshall and Gilligan, 1993). A significant contrast in rheology exists between sulfide minerals and silicate and carbonate host rocks at low metamorphic grades, with the common sulfides (galena, pyrrhotite, sphalerite, chalcopyrite) being less competent than silicate and carbonate host rocks, while pyrite and magnetite are more competent (Marshall and Gilligan, 1993; Rosière et al., 2001). The Kettara pyrrhotite-rich massive sulfide lens is less competent than the surrounding wall rocks and this difference in mechanical behavior should lead to concentration of deformation in the weaker material (pyrrhotite ore body), with possible fracturing and boudinage of the more competent material and shear-strain concentrated along ore-host rock contacts. Such deformation partitioning is not observed at Kettara. On the contrary, pyrrhotite truncates the S1 cleavage (Fig. 4E), and the ore contacts are controlled by fracture and cleavage directions, suggesting replacement of the host rock, while cleavage was overprinted by pyrrhotite and associated sulfides. Such syntectonic replacement could potentially be attributed to redistribution in and around a precursor ore body by local dissolution and precipitation processes (remobilization). However if the main part of the sulfides were pre-tectonic, the more competent sulfide minerals should be boudinaged in a softer matrix of different composition (Gilligan and Marshall, 1987; Aerden, 1994), and pressure shadows should develop around rigid objects like pyrite and magnetite crystals (Passchier and Trouw, 1996; Ramsay and Lisle, 2000). No such evidence is seen at Kettara. In addition, the microstructural control and the progressive gradation from wall rocks-rich ore (semi massive pyrrhotite) to texturally identical wall rocks-poor ore (massive pyrrhotite) suggests that massive ore differs from semi massive ore by the extent of replacement only (Perkins, 1997; De Roo, 1989; Aerden, 1994). Following the guidelines of Marshall and Gilligan (1993), the microstructures at Kettara show little evidence for solid-state mechanical remobilization of original sulfides.

7.3. Emplacement of the Kettara massive sulfide deposit

The fluid inclusion compositions presented here for both the mineralized veins adjacent to the deposit and the shear zones-related veins in the intrusion are compatible with mixing of magmatic and metamorphic fluids. This is supported by the oxygen and hydrogen isotope data for chlorite and quartz from these veins, and aligns well with field and microstructural relationships, which clearly indicate that the veins were formed during deformation and metamorphism. The oxygen and hydrogen isotopic composition of quartz and chlorite in the mineralized veins adjacent to the deposit are similar to those of quartz and chlorite from the shear zones cutting across the Kettara intrusion and support interaction with the same hydrothermal fluid. Calculated hydrogen and oxygen isotope compositions clearly demonstrate involvement of metamorphic water in both the mineralized veins adjacent to the deposit and the shear zones cutting across the intrusion (Fig. 7). The field, microstructural, isotope and fluid inclusion evidence clearly link the hydrothermal alteration around the Kettara deposit and intrusion, including the formation of the mineralized veins, to a fluid flow focused along the Kettara shear zone. The difference recorded in fluid inclusions composition between the unmineralized and mineralized veins can be related to migration of metamorphic fluids through the interconnected regional shear zones into host rocks rich in organic matter where their reduction contributed to precipitation of sulfides. Crystallization of pyrrhotite instead of pyrite in the mineralized veins probably arises from the organic-matter driven reducing conditions during metamorphism as has been observed in graphitic sulfide-rich schists from south-central Maine (Ferry, 1981) and Late Precambrian Lower Dalradian Ballachulish Slate Formation metasediments (Hall et al., 1987).

The major question that remains is the relationship of this syn-metamorphic hydrothermal episode to the formation of the Kettara massive sulfide deposit. The deformational history of many massive sulfide deposits within the Variscan belt has been a subject of much debate (e.g. Marignac and Cathelineau, 2006; Sanchez-Espana et al., 2006; Marcoux et al., 2008; Essaifi and Hibti, 2008) between proponents of syngenetic versus epigenetic models.

At Kettara, the mineralized veins may hold the key to answering this question. The presence of sulfides within the mineralized veins indicates a genetic relationship with the deposit, but does not yet prove that they formed at the same time. The mineralized veins could have derived their sulfide content by syntectonic remobilization (dissolution and reprecipitation) of a preexisting syngenetic massive sulfide deposit. However, the textural evidence for syntectonic sulfide replacement of foliated host rock plus the structurally controlled localization of the deposit in a step-zone between regional shear zones favor a model in which veins and massif sulfides formed synchronously from the same fluid. It could still be argued in this case that this deformation episode completely remobilized an earlier syngenetic massive sulfide deposit, but although no field or textural evidence remains to support this hypothesis. The 331 and 300 Ma ages obtained for alteration minerals around similar deposits in Central Jebilet and Guemassa massifs (Marcoux et al., 2008; Watanabe, 2002) support emplacement of these massive sulfide deposits during regional deformation metamorphism.

Late-stage pyrite and carbonate veins within the Kettara shear zone are only affected by brittle deformation, clearly indicating that metal-bearing hydrothermal fluids continued to circulate in the Kettara area as deformation evolved from ductile to brittle conditions. Formation of the Kettara mineralized veins was thus realized through a protracted period of deformation and sulfide mineralization.

8. Conclusion

Central Jebilet represents a major massive sulfide province of significant economic importance. The clear association of the massive sulfide deposits with bimodal magmatism and shear zones is exemplified in the Kettara area where a massive sulfide deposit and a mafic-ultramafic intrusion are located within a "compressional jog" of a regional wrench shear zone. Field and textural evidence clearly indicate that mineralized veins adjacent to the deposit developed during shearing, and that hydrothermal fluid circulation continued into the brittle deformation regime. Hydrothermal alteration in both the intrusion and the wall rocks adjacent to the deposit are similar and related to the same hydrothermal fluids, i.e. a mixture of metamorphic H_2O - (CO_2, N_2, CH_4) and magmatic fluids (H_2O-Salt). We conclude that if the mineralized veins are an integral part of the Kettara deposit, then emplacement of the pyrrhotite-rich massive sulfide deposit occurred during deformation and metamorphism. The metamorphic fluids scavenged sulfur and metals from the country rocks and were channeled through active shear zones, depositing massive sulfides in reducing environments offered by organic-rich host rocks. The alternative interpretation that the mineralized veins represent remobilization products of a pretectonic orebody is possible but not supported by our data for Kettara. Further work is undoubtedly needed to assess mineralization models at the scale of the whole central Jebilet.

Acknowledgements

This work received a financial support from the project URAC43. A. Mouttaqi from ONHYM an M. Zouhair, A. Ouadjou and A. Radnaoui from MANAGEM are thanked for making documents and drill cores of the deposit available for study. Thanks also to P. Lusty from BGS for critical reading of the manuscript. Constructive comments and suggestions by Domingo Aerden, which improved the presentation of data and the discussion, were highly appreciated.

References

Aarab, E.M., 1984, Mise en évidence du caractère co-génétique des roches magmatiques basiques et acides dans la série volcano-sédimentaire de Sarhlef (Jebilet, Maroc Hercynien): Unpublished 3rd cycle thesis, Nancy University, Nancy, 124p.

Aerden, A. G. A. M., 1994, Microstructural timing of the Rosebery massive sulfides, Tasmania: evidence for a metamorphic origin through mobilization of disseminated base metals: Journal of metamorphic Geology, v.12, p. 505-522.

Agard, J., Destombes, J., and Van Leckwijck, W., 1952, Géologie de gîtes minéraux marocains, Fer: Notes et Mémoires du Service Géologique du Maroc, v. 87, p. 128-128.

Ait-Tahar, M., 1987, Géométrie et cinématique de la déformation post-viséenne autour des gabbros des Jebilet, l'exemple des gabbros de Kettara et de Jbel El-Harcha-Massif hercynien des Jebilet-Maroc: Unpublished 3rd cycle thesis, Cadi Ayyad university, Marrakech, 144 p.

Beauchamp, J., 1984, Le carbonifère inférieur des Jebilet et de l'Atlas de Marrakech (Maroc) : migration et comblement d'un bassin marin: Bulletin de la Société Géologique de France, v. 7, p. 1025-1032.

Beauchamp, J., and Izart, A., 1987, Early Carboniferous basins of the Atlas-Meseta domain (Morocco): Sedimentary model and geodynamic evolution: Geology, v. 15, p. 797-800.

Beauchamp, J., Izart, A., and Piqué A., 1991, Les bassins d'avant pays de la chaîne hercynienne au carbonifère inférieur: Canadian Journal of Earth Sciences, v. 28, p. 2024-2041.

Belkabir, A. Gibson, H.L., Marcoux., E., Lentz, D., and Rziki, S., 2008, Geology and wall rock alteration at the Hercynian Draa Sfar Zn–Pb–Cu massive sulfide deposit, Morocco: Ore Geology Review, v. 33, p. 280-306.

Bellot, J.P., 2004, Shear zone-hosted polymetallic sulfides in the south Limousin area, Massif Central, France: Remobilized sulfides deposits related to Variscan collision tectonics and amphibolite metamorphism: Economic Geology, v. 99, p. 819-827.

Ben Abbou, M., Soula, J.C.,Brusset, S.,Roddaz, M., Ntarmouchant, A., Driouch, Y., Christophoul, F., Bouabdelli, M., Majesté-Menjoulas, C., Beziat, D., Debat, P., Deramond, J., 2001, Contrôle tectonique de la sédimentation dans le système de bassins d'avant-pays de la Meseta marocaine: Comptes Rendus de l'Académie des Sciences de Paris, v. 332, p. 703–709.

Bernard, A.J., Maier, O.W., and Mellal, A., 1988, Aperçu sur les amas sulfurés massifs des hercynides Marocaines: Mineralium Deposita, v. 23, p. 104-114.

Bernardin, C., 1988, Interprétation gravimétrique et structure profonde de la Meseta marocaine et de sa marge atlantique : Unpublished Ph. D. thesis, Marseille University, France.

Berthé, D., Choukroune, P., and Jegouzo, P., 1979, Orthogneiss, mylonite, and non-coaxial deformation of granite: the example of South Armorican shear zone: Journal of Structural Geology, v. 1, p. 31-42.

Bodnar, R.J., 2003, Introduction to Fluid Inclusions, *in* Samson, L., Anderson, A., Marshal, D. Eds., Fluid Inclusions: Analysis and Interpretation: Mineralogical Association of Cananda Short Course 32, p. 1-8.

Bodnar, R.J., and Vityk, M.O., 1994, Intrepretation of microthrermometric data for H2O-NaCl fluid inclusions. In: De Vivo B, Frezzotti ML (eds) Fluid Inclusions in Minerals, Methods and Applications: Virginia Tech, Blacksburg, VA, 17-130.

Bordonaro, M., 1983, Tectonique et pétrographie du district à pyrrhotite de Kettara (Paléozoïque des Jebilet, Maroc): Unpublished 3rd cycle thesis, Université Louis Pasteur, Strasbourg, 132p.

Bouabdelli, M., and Piqué, A., 1996, Du bassin sur décrochement au bassin d'avant-pays: Dynamique du bassin d'Azrou-Khénifra (Maroc hercynien central): Journal of African Earth Sciences, v. 23, p. 213–224.

Bouchot, V., Milesi, J.P., and Ledru, P., 2000, Crustal-scale hydrothermal palaeofield and related Au, Sb, W orogenic deposits at 310–305 Ma (French Massif Central, Variscan belt): Society of Geology Applied to Ore Deposits, SGA News, v. 10, p. 6–12.

Boulin, J., Bouabdelli, M., and El Houicha, M., 1988, Evolution paléogéographique et géodynamique de la chaîne Paléozoïque du Moyen- Maroc: Un essai de modélisation: Comptes Rendus de l'Académie des Sciences de Paris, v. 306, p. 1501–1506.

Brown, D., and McClay, K.R., 1993, Deformation textures in pyrite from the Vangorda Pb-Zn-Ag deposit, Yukon, Canada: Mineralogical Magazine, v. 57, p. 55-66.

Burkhard, M., Caritg, S., Helg, U., Robert-Charrue, C., and Soulaimani, A., 2006, Tectonics of the Anti-Atlas of Morocco: Comptes Rendus Geoscience, v. 338, p. 11-24.

Chernicoff, C.J., Richards, J.P., and Zappettini, E.O., 2002, Crustal lineament control on magmatism and mineralization in northwestern Argentina: Geological, geophysical, and remote sensing evidence: Ore Geology Reviews, v. 21, p. 127–155.

Chopin, F., Corsini, M. Schulmann, K. El Houicha, M. Ghienne, J.-F., Edel J.-B., 2014, Tectonic evolution of the Rehamna metamorphic dome (Morocco) in the context of the Alleghanian- Variscan orogeny: Tectonics, v. 33, p. 1154–1177.

Cole, D.R., Ripley, E.M., 1998, Oxygen isotope fractionation between chlorite and water from 170 to 350°C: a preliminary assessment based on partial exchange and fluid/rock experiments: Geochimica et Cosmochimica Acta, v. 63, p. 449–457.

Coomer, P.G., Robinson, B.W., 1976, Sulfur and sulphate-oxygen isotopes and the origin of the Silver mines deposits, Ireland: Mineralium Deposita, v. 11, p. 155-169.

Cox, S.F., Wall, V.J., Etheridge, M.A., and Potter, T.F., 1991, Deformation and metamorphic processes in the formation of mesothermal vein-hosted gold deposits-examples from the Lachlan fold belt in central Victoria, Australia: Ore Geology Reviews, v. 6, p. 391–423.

Cox, S.F., Knackstedt, M.A., and Braun, J., 2001, Principles of structural control on permeability and fluid flow in hydrothermal systems: Reviews in Economic Geology, v. 14, p. 1–24.

De Roo, J. A., 1989, The Elura Ag-Pb-Zn mine in Australia_ore genesis in a slate belt by syndeformational metasomatism along hydrothermal fluid conduits: Economic geology, v. 84, p. 256-278.

Essaifi, A., 1995, Relations entre magmatisme, déformation et altération hydrothermale, l'exemple des Jebilet centrales (hercynien, Maroc): Mémoires Géosciences Rennes, 66.

Essaifi, A., Capdevila, R., and Lagarde, J.L., 1995, Transformation de leucogabbros en chloritoschistes sous l'effet de l'altération hydrothermale et de la déformation dans l'intrusion de Kettara (Jebilet centrales): Comptes Rendus de l'Académie des Sciences de Paris, v. 320, p. 189-196.

Essaifi, A., Lagarde, J.L., and Capdevila, R., 2001, Deformation and displacement from shear zone patterns in the Variscan upper crust, Jebilet, Morocco: Journal of African Earth Sciences, v. 32, p. 335-350.

Essaifi, A., Potrel, A., Capdevila, R., Lagarde, J.L., 2003, Datation U-Pb: âge de mise en place du magmatisme bimodal des Jebilet centrales (chaîne Varisque, Maroc): Comptes Rendus Geoscience, v. 335, p. 193-203.

Essaifi, A., Capdevila, R., Fourcade, S., Lagarde, J.L., Ballevre, M., and Marignac, C., 2004, Hydrothermal alteration, fluid flow and volume change in shear zones: the layered mafic-ultramafic Kettara intrusion (Jebilet Massif, Variscan belt, Morocco): Journal of Metamorphic Geology, v. 22, p. 25-43.

Essaifi, A., and Hibti, M., 2008, The hydrothermal system of Central Jebilet (Variscan Belt, Morocco): A genetic association between bimodal plutonism and massive sulfide deposits?: Journal of African Earth Sciences, v. 50, p. 188-203.

Essaifi, A., 2011, L'ancienne mine de pyrrhotine de Kettara: Notes et Mémoires du Service Géologique du Maroc, v. 563, p. 71-82.

Essaifi, A., Samson, S., and Goodenough, K., 2014, Geochemical and Sr-Nd isotopic constraints on the petrogenesis and geodynamic significance of the Jebilet magmatism (Variscan Belt, Morocco): Geological Magazine, v. 151, p. 666-691.

Ferry, J. M., 1981, Petrology of graphitic sulfide-rich schists from south-central Maine: an example of desulfidation during prograde regional metamorphism: American Mineralogist, v. 66, p. 908-930.

Fournier, M., Felenc, J., and Hmeurras, M., 1987, Un amas sulfuré à pyrrhotine en milieu sédimentaire Kettara (Jebilet, Maroc): rapport du Bureau des Recherches Géologiques et Minières, 86 MAR 165, 77p.

Gaouzi, A., Chauvet, A., Barbanson, L., Lakhlifi, B., Touray, J.C. Oukarrou, S., and El Wartiti, M., 2001, Mise en place syntectonique des minéralisations cuprifères du gîte d'Ifri (district du Haut Seksaoua, Haut Atlas occidental, Maroc): Comptes Rendus de l'Académie des Sciences de Paris, v. 333, p. 277–284.

Gates, A.E., and Speer, J.A., 1991, Allochemical retrograde metamorphism in shear zones: an example in metapelites, Virginia, USA: Journal of Metamorphic Geology, v. 9, p. 581–604.

Gilligan, L.B., and Marshall, B., 1987, Textural evidence for remobilization in metamorphic environments: Ore Geology Reviews, v. 2, p. 205-229.

Glazner, A.F., 1991, Plutonism, oblique subduction, and continental growth: An example from the Mesozoic of California: Geology, v. 19, p. 784–786.

Glen, R. A., 1987, Copper- and gold-rich deposits in deformed turbidites at Cobar, Australia : their structural control and hydrothermal origin: Economic Geology, v. 82, p.124-140

Goldstein, R.H., and Reynolds, T.J., 1994. Systematics of fluid inclusions in diagenetic minerals: SEPM Short Course 31.

Groves, D.I., Goldfarb, R.J., Gebre-Mariam, M., Hagemann, S.G., and Robert, F., 1998, Orogenic gold deposits: A proposed classification in the context of their crustal distribution and relationship to other gold deposit types: Ore Geology Reviews, v. 13, p. 7–27.

Hall, A.J., Boyce, A.J., and Fallick, A.E., 1987, Iron sulfides in metasediments: isotopic support for a retrogressive pyrrhotite to pyrite reaction: Chemical Geology, v. 65, p. 305-310.

Hedenquist, J.W., and Lowenstern, J.B., 1994, The role of magmas in the formation of hydrothermal ore deposits: Nature, v. 370, p. 519–527.

Hibti, M., 2001, Les amas sulfurés des Guemassa et des Jebilet (Meseta Sud-Occidentale, Maroc). Témoins de l'hydrothermalisme précoce dans le bassin mesetien : Thèse de Doctorat d'Etat Es-Sciences, Université Cadi Ayyad, Marrakech, 318p.

Hibti, M., and Marignac, C., 2001, The Hajjar deposit of Guemassa (SW Meseta, Morocco): a metamorphosed syn-sedimentary massive sulfide ore body of the Iberian type of volcano-sedimentary massive sulfide deposits, *in* Piestrzynski A et al. eds. Mineral Deposits at the Beginning of the 21st Century, p. 281-284

Hoepffner, C., Soulaimani, A., and Piqué, A., 2005, The Moroccan Hercynides. Journal of African Earth Sciences, v. 43, p. 144-165.

Hoepffner, C., Houari, M.R., and Bouabdelli, M., 2006, Tectonics of the North African Variscides (Morocco, Western Algeria), an outline: Comptes Rendus Geoscience, v. 338, p. 25-40.

Hollard, H., 1978, L'évolution hercynienne au Maroc : Zeitschrift Deutsche Géologie Gesellschaft, v. 129, p. 495-512.

Holloway J.R., 1984, Graphite-CH_4-H_2O-CO_2 equilibria at low-grade metamorphic conditions: Geology, v. 12, p. 455-458

Huvelin, P., 1970, Amas stratiforme de pyrrhotine dans les schistes carbonifères du district des gabbros de Kettara (Jebilet, Maroc): Comptes Rendus de l'Académie des Sciences de Paris, v. 270, p. 2517-2520.

Huvelin, P., 1972. Carte géologique et des minéralisations des Jebilet centrales au 1/100 000: Notes et Mémoires du Service Géologique du Maroc, v. 232a.

Huvelin, P., 1977, Etude géologique et gîtologique du massif hercynien des Jebilet (Maroc occidental): Notes et Mémoires Service Géologique du Maroc, v. 232 bis, p. 1-307.

Huvelin, P, and Permingeat, F., 1980, Soufre, pyrite, pyrrhotite: Notes et Mémoires du Service Géologique du Maroc, v. 276, p. 227-243.

Jadid, M., 1989, Etude des processus de différenciation des roches magmatiques pré-orogéniques des Jebilet centrales sur l'exemple du massif stratiforme de Koudiat Kettara (Maroc Hercynien): Unpublished 3rd cycle thesis, Cadi Ayyad University, Marrakech.

Kamona, F, 2011, Carbonate-Hosted Base Metal Deposits, *in* Dr. Imran Ahmad Dar eds., Earth and Environmental Sciences, p. 393-422.

Kharbouch, F., Juteau, T., Treuil, M., Joron, J.L., Piqué, A., Hoepffner, C., 1985. Le volcanisme dinantien de la Meseta marocaine nord-occidentale et orientale; caractères pétrographiques et géochimiques et implications géodynamiques. Sciences Géologiques Bulletin Strasbourg, v. 38, p. 155–163.

Lacroix, B., and Vennemann, T., 2015, Empirical calibration of the oxygen isotope fractionation between quartz and Fe–Mg-chlorite. Geochimica et Cosmochimica Acta, 149, p. 21-31

Lagarde J. L., and Choukroune, P., 1982, Cisaillement ductile et granitoïdes syntectoniques : l'exemple du massif hercynien des Jebilet (Maroc). Bulletin de la Société Géologique de France, v. 24, p. 299-307.

Lagarde, J. L., and Michard, A., 1986, Stretching normal to the regional thrust displacement in a thrust-wrench shear zone, Rehamna massif, Morocco: Journal of Structural Geology, v. 8, p. 483–492.

Lagarde J. L., Aït Omar, S, and Roddaz, B., 1990, Structural characteristics of syntectonic plutons with special reference to late carboniferous plutons from Morocco: Journal of Structural Geology, v. 12, p. 805-821.

Lawrence, D.M., Treloar, P.J., Rankin, A.H., 2013, A fluid inclusion and stable isotope study at the Loulo Mining Distrct, Mali, West Africa: Implications for multifluid source in the generation of orogenic gold deposits: Economic Geology, v.108, p. 229-257.

Leach, D. L., Sangster, D. F., Kelley, K. D., Large, R. R., Garven, G., Allen, C. R., Gutzmer, J., and Walters, S., 2005, Sediment-Hosted Lead-Zinc Deposits: A Global Perspective: Economic Geology 100th Anniversary volume, p. 561–607.

Le Corre, C., and Bouloton, J., 1987, Un modèle de ‘‘structure en fleur’’ associant décrochement et convergence: Les Jebilet centro-occidentales (Maroc hercynien) : Comptes Rendus de l’Académie des Sciences de Paris, v. 13, p. 751-755

Le Corre, C., and Saquaque, A., 1987, Comportement d'un système pluton-encaissant dans un champ de déformation régional : le granite de Bramram (Jebilet, Maroc hercynien): Bulletin Société Géologique France, v. 4, p. 665-673.

Leblanc, M., 1993, Amas sulfuré formé par injection de sills dans des sédiments : exemple d'Hajjar (Marrakech, Maroc): Comptes Rendus de l’Académie des Sciences de Paris, v. 316, p. 499-504.

Leclère, H., Lacroix, B., Fabbri, O., 2014, Fault mechanics at the base of the continental seismogenic zone: Insights from geochemical and mechanical analyses of a crustal-scale transpressional fault from the Argentera crystalline massif, French–Italian Alps: Journal of Structural Geology**,** v. 66, p. 115–128.

Lotfi, F., Belkabir, A., Brown, A.C., Marcoux, E., Brunet, S., and Maacha, L., 2008, Geology and Mineralogy of the Hercynian Koudiat Aïcha Polymetallic (Zn-Pb-Cu) Massive Sulfide Deposit, Central Jebilet, Morocco: Exploration and Mining Geology, v. 17, p. 15-31.

Lotfi, F., Belkabir, A., Brunet, S., Brown, A.C., and Marcoux, E., 2010, Lithogeochemical, mineralogical analyses and oxygen–hydrogen isotopes of the Hercynian Koudiat Aïcha massive sulfide deposit, Morocco: Journal of African Earth Sciences, v.5, p. 150–166.

Marcoux, E., Belkabir, A., Gibson, H.L., Lentz, D., and Ruffet, G., 2008, Draa Sfar, Morocco: A Visean (331 Ma) pyrrhotite-rich, polymetallic volcanogenic massive sulfide deposit in a Hercynian sediment dominant terrane: Ore Geology Reviews, v. 33, p. 307-328.

Marignac, Ch., and Cathelineau, M., 2006, Comment on the paper by Sanchez-Espana et al.: source and evolution of ore-forming hydrothermal fluids in the northern Iberian pyrite belt massive sulphide deposits (SW Spain): evidence from fluid inclusions and stable isotopes (Mineralium Deposita 38: 519–537): Mineralium Deposita, v. 40, p. 742–748.

Marshall, B., and Gilligan, L. B., 1993, Remobilization, syn-tectonic processes and massive sulfide deposits: Ore Geology Reviews, v. 8, p. 39-64

Marshall, B., and Spry, P. G, 2000, Discriminating between regional metamorphic remobilization and syntectonic emplacement in the genesis in the massive sulfide ores: Reviews in Economic Geology, v. 11, p. 39-80.

Mayol, S., and Muller, J., 1985, Mise en évidence d'une unité allochtone hercynienne précoce (antéschisteuse) dans les Jebilet occidentales (Maroc). Etude de structuration de la zone de contact: Comptes Rendus de l'Académie des Sciences de Paris, v. 300, p. 369-372.

Michard, A., Soulaimani, A., Hoepffner, C., Ouanaimi, H., Baidder, L., Rjimati, E.C., and Saddiqi, O., 2010, The South-Western Branch of the Variscan Belt: Evidence from Morocco: Tectonophysics, v. 492, p. 1-24.

Moreno, C., Sáez, R., González, F., Almodóvar, G., Toscano, M., Playford, G., Alansari, A., Rziki, S., and Bajddi, A., 2008, Age and depositional environment of the Draa Sfar massive sulfide deposit, Morocco: Mineralium Deposita, v. 43, p. 891-911.

Mrini, Z., Rafi, A., Duthou, J. L. and Vidal, P., 1992, Chronologie Rb-Sr des granitoïdes hercyniens du Maroc : conséquences: Bulletin de la Société Géologique de France, v. 163, p. 281-291.

Nicol, N., Legendre, O., and Charvet, J., 1997, Les minéralisations Zn-Pb de la série paléozoïque de Pierrefite (Hautes-Pyrénées) dans la succession des événements tectoniques hercyniens: Comptes Rendus de l'Académie des Sciences de Paris, v. 324, p. 453–460.

Oliver, N.H.S., 1996, Review and classification of structural controls on fluid flow during regional metamorphism: Journal of Metamorphic Geology, v. 14, p. 477–492.

Passchier, C. W., and TROUW, R. A. J., 1996, Microtectonics. Heidelberg: Springer-Verlag, 289 p.

Perkins, W. G., 1997, Mount Isa lead-zinc orebodies: Replacement lodes in a zoned syndeformational copper-lead zinc system: Ore Geology Review, v. 12, p. 61-110.

Piessens, K., Muchez, Ph., Dewaele, S., Boyce, A., De Vos, W., Sintubin, M., Debacker, T.N., Burke, E.A.J., and Viaene, W., 2002, Fluid flow, alteration and polysulfide mineralisation associated with a low-angle reverse shear zone in the Lower Palaeozoic of the Anglo-Brabant fold belt, Belgium: Tectonophysics, v. 348, p. 73–92.

Piqué, A., and Michard, A., 1989, Moroccan hercynides, a synopsis. The paleozoic sedimentary and tectonic evolution at the northern margin of West Africa: American Journal of Sciences, v. 298, p. 286–330.

Piqué, A., Jeannette, D., and Michard, A., 1980, The Western Meseta shear zone, a major and permanent feature of the Hercynian belt of Morocco: Journal of Structural Geology, v. 2, p. 55-61.

Poty, B., Leroy, J., Jachimowicz, L., 1976, Un nouvel appareil pour la mesure de des températures sous le microscope : l'installation de microthermométrie Chaixmeca: Bulletin de la Société Française de Minéralogie et de Cristallographie, v. 9, p. 182-186.

Ramsay, J. G., and Lisle, R. J., 2000, The techniques of modern structural geology, Vol. 3: Applications of continuum mechanics in structural geology: London Academic Press, p. 702–1061.

Robinson, B.W., and Kusakabe, M., 1975, Quantitative preparation of SO_2 for $^{34}S/^{32}S$ analysis from sulfides by combustion with cuprous oxide: Analytical Chemistry, v. 47, p. 1179-1181.

Roddaz, M., Brusset, S., Soula, J.C., Beziat, D., Ben Abbou, M., Debat, P., Driouch, Y., Christophoul, F., Ntarmouchant, A., and Deramond, J., 2002, Foreland basin magmatism in the western Moroccan Meseta and geodynamic inferences: Tectonics, v.21, p. 1043–1065

Roddaz, M., Soula, J.C., Ben Abbou, M.B., Brusset, S., Debat, P., Ntarmouchant, A., Driouch, Y., and Béziat, D., 2006, Comment on “The Moroccan Hercynides” by Hoepffner et al. (Journal of African Earth Sciences, v. 43, p. 144–165): Journal of African Earth Sciences, v. 45, p. 515–517.

Roedder, E., 1984, Fluid inclusions: Reviews in Mineralogy 12. Mineralogical Society of America, 646 p.

Rosière, A., Siemes, H., Quade, H., Brokmeier, H.G. and Jansen, E. M., 2001, Microstructures, textures and deformation mechanisms in hematite: Journal of Structural Geology, v. 23, p. 1429–40.

Ruano S.M., 2008, Analytical techniques applied to fluid inclusion studies: basics and applications. In: Subías I, Bauluz B (eds) Tech. Appl. To Miner: Geochemistry Seminarios, Spain, p. 133-154.

Sanchez-Espana, J., Velasco, F., Boyce, A. J, and Tornos, F., 2006, Reply to the comments by Marignac and Cathelineau on the paper by Sanchez-Espana et al.: Source and evolution of ore-forming hydrothermal fluids in the northern Iberian Pyrite Belt massive sulfide deposits (SW Spain): evidence from fluid inclusions and stable isotopes (Mineralium Deposita 38: 519–537): Mineralium Deposita, v. 40, p. 749–754.

Segall, P., and Simpson, C., 1986, Nucleation of ductile shear zones on dilatant fractures: Geology, v. 14, p. 56–59

Shepherd, T.J., Rankin, A.H., and Alderton, D.H.M., 1985, A practical guide to fluid inclusion studies: Blackie and Sons Ltd, Glasgow.

Sheppard, M.F., 1986, Characterization and isotopic variations in natural waters, *in* Valley et al. eds., Stable Isotopes in High Temperature Geological Processes, Reviews in Mineralogy: Mineralogical Society of America, v. 16, p. 165-183.

Sibson, R.H., Robert, F., and Poulsen, K.H., 1988, High-angle reverse faults, fluid pressure cycling and mesothermal gold– quartz deposits: Geology, v. 16, p. 551-555.

Sillitoe, R.H., 2000, Gold-rich porphyry deposits: descriptive and genetic models and their role in exploration and discovery: Society of Economic Geologists Review, v. 13, p. 315-345.

Simoneit, B. R., Grimalt, J. O., Hayes, J. M., and Hartman, H., 1987, Low temperature hydrothermal maturation of organic matter in sediments from the Atlantis II Deep, Red Sea: Geochimica et cosmochimica acta, v. 51, p. 879-894.

Souaré, A. T., 1988, Contribution à l'étude des amas sulfurés du district des Jebilet centrales et de leurs altérations supergènes (chapeau de fer). Comparaison avec les minéralisations sulfurées d'Agouim (Haut Atlas, Maroc): Unpublished 3rd cycle thesis, Cadi Ayyad University, Marrakech.

Taylor, H. P. J., 1974, The application of oxygen and hydrogen isotope studies to problems of hydrothermal alteration and ore deposition: Economic Geology, v. 69, p. 843-883.

Thiéry, R., Vidal, J., and Dubessy, J., 1994, Phase equilibria modelling applied to fluid inclusions: Liquid-vapour equilibria and calculation of the molar volume in the CO_2-CH_4-N_2 system: Geochimica et Cosmochimica Acta, v. 58, p. 1073-1082.

Van den Kerkhof, A.M., and Hein, U.F., 2001, Fluid inclusion petrography: Lithos, v. 55, p. 27-47.

Velasco, F., Sánchez-España, J., Boyce, A.J., Fallick, A.E., Sáez, R., and Almodóvar, G.R., 1998, A new sulfur isotopic study of some Iberian Pyrite Belt deposits: evidence of a textural control on sulfur isotope composition: Mineralium Deposita, v. 34, p. 4-18.

Wan, B., Zhang, L., Xiao, W., 2010, Geological and geochemical characteristics and ore genesis of the Keketale VMS Pb–Zn deposit, Southern Altai Metallogenic Belt, NW China: Ore Geology Reviews, v. 37, p. 114-126.

Watanabe, Y., 2002, $^{40}Ar/^{39}Ar$ Geochronology constraint on the timing of massive sulfide and vein-type Pb-Zn Mineralization in the Western Meseta of Morocco: Economic Geology, v. 97, p. 145-157.

Weber, K., 1981, Kinematic and metamorphic aspects of cleavage formation in very low-grade metamorphic slates: Tectonophysics, v. 78, p. 291-306.

Zheng, Y.F., 1993, Calculation of oxygen isotope fractionation in hydroxyl-bearing silicates. Earth and Planetary Science Letters, v. 120, p. 247–263.

Figure Captions

Fig. 1A) The Jebilet massif in the framework of the Palaeozoic outcrops of North Africa (in grey), B) Location of the Jebilet massif in the frame of the Variscan fold belt of Morocco, C) Geological sketch map of the Jebilet massif (modified after Huvelin 1977). Box encloses area covered by Figure 2.

Fig. 2 A) Shear zone pattern in Central Jebilet (modified after Essaifi and Hibti, 2008), B) Schistosity trajectories and deformation kinematics around the Oled Har-Kettara-Safsafat magmatic lineament. Regional schistosity displays curvatures that indicate N-S sinistral wrenching interconnected by an east-northeast dextral shear zone in the Kettara area, C) Geological and structural map of the Kettara area. Location of the cross-section shown in Fig. 3 is indicated.

Fig. 3 Vertical cross-section through the Kettara intrusion and Cu deposit. See location in Fig. 2C. The diagrammatic sections illustrate meter-scale shear zones in the Kettara mafic-ultramafic intrusion and the relationships between deformation and quartz ±calcite veins in both the intrusion and the gossan. Stereographic diagrams show equal area, lower hemisphere projections of planar and linear structures. S0 (bedding) and Le (stretching lineation) in the Kettara intrusion were measured respectively at the bottom of the intrusion and in the contact aureole around the intrusion. The S1 stereonet represents the regional schistosity in the whole Kettara area.

Fig. 4 Representative field exposures of the Kettara intrusion and deposit and drill core specimen of the Kettara deposit. A) Panoramic view from the Kettara intrusion, looking northwest to the Kettara deposit, and showing the relief of the Kettara gossan and the remnants of old workings, B) Mineralized quartz-chlorite vein cutting the schists at a low angle in the Kettara gossan, C) Quartz mineralized vein crosscutting wall rocks composed of alternating pelites (black) and sandstone (grey) layers. Note that mineralization within the vein lie in continuity with the pelite layers., D) Sigmoidal quartz-calcite vein in a chlorite-rich shear zone of the Kettara intrusion, E) Specimen from the drill core K101 showing the contact between the pyrrhotite lens and the host schists. Pyrrhotite (PO) cuts across the contact, contains enclaves of the host schists (HS) and is crosscut by carbonate (CC) veins, (F) Specimen from the drill core K101showing a mineralized quartz-chlorite vein crosscut by a carbonate (CC) vein (scale piece is 24 cm across).

Fig. 5 Photomicrographs of the Kettara ore and its host rocks. A) Metapelites located 170 m to the south of the deposit, showing the stratification (S_0) and schistosity (S_1) planes, B)Chloritized metapelites located 2m from the southern boundary of the deposit, showing pressure shadows around ilmenitegrains (Ilm), c) Semi-massive pyrrhotite ore showing chloritized wall rocks with S_1 cleavage truncated by pyrrhotite, D) polymetallic assemblage of pyrrhotite, chalcopyrite (Ccp), sphalerite (Sph), arsenopyrite (Asp) replaced by carbonates (Car), E) replacement of a pyrrhotite-chalcopyrite assemblage by carbonates and euhedral pyrite (Py), F) Cataclastic deformation of pyrite resulting in comminution breccias.A, B (transmitted light), C, D, E, F (reflected light).

Fig. 6 Paragenetic successions of the main mineralizing fluids in the Kettara massive sulfide deposit. 1 and 2 are respectively the first (pyrrhotitic ore) and the second (pyritic ore) main phases of mineralization

Fig. 7 Plot of δD vs. δ^{18}O values of chlorite (white star) and the calculated mineralizing fluid (white square). Fluid composition was calculated using oxygen and hydrogen fractionation between chlorite and water from Zheng (1993) and Cole and Ripley (1998) for oxygen, and from Graham et al. (1987) for hydrogen. Compositions of Primary igneous water, metamorphic water and sedimentary rocks are from Sheppard (1986).

Fig. 8 Photomicrography and sketch of some fluid inclusions in quartz-chlorite veins of the Kettara intrusion. A) Assemblage of aquo-carbonic (H_2O-CO_2-Salt) fluid inclusions composed by two phases and three phases (L, V1, V2) fluid inclusions (type 1). B) sketch showing an aqueous-saline (H_2O+Salt) fluid inclusions, composed by two phases and three phases (S, L, V) primary (I) and secondary (II) fluid inclusion plans of type 3. C) two phases aqueous-saline fluid inclusions of type 3 (I) showing irregular shapes and oriented along the elongation of quartz crystal (photomicrography of the central part in B).

Fig. 9 Photomicrography of main fluid inclusions in quartz (A-D) and calcite (E) of quartz-calcite vein of the Kettara intrusion. A) two phases H_2O-N_2-CH_4 fluid inclusions (type 4). B) One phase CO_2-N_2-CH_4primary fluid inclusions (type 2 (I)). C) Intragranular plans of two phases aqueous fluid inclusions (type 5). D) Assemblageof secondary fluid inclusion plans including one phase CO_2-N_2-CH_4 fluid inclusions (type 2 (II)) and two phases fluid inclusions (type 5). E) Aqueous fluid inclusions (type 5) in calcite, which is considered as secondary with respect to the vein formation.

Fig. 10 Histogram frequency of microthermometric data of fluid inclusions in veins from the shear zones of the Kettara mafic ultra-mafic intrusion. (a-b) $T_{m(CO2)}$ (a) and $T_{h(CO2)}$ (b) of aqueous gas-bearing fluid inclusions (type 1). (c-d) $T_{m(ice))}$ (c) and T_h (d) of aqueous gas-bearing fluid inclusions (type 1 and type4). (e-f) $T_{m(CO2)}$ (e) and $T_{h(CO2)}$ (f) of aqueous gas-rich fluid inclusions (type 2). Homogenization occurs either into liquid phase (l) or vapor phase (v), as critical (c) or decrepitation(*d*). V_{qcl} : quartz-chlorite veins, V_{qcc}: quartz-calcite vein.

Fig. 11 Histogram frequency of microthermometric data of fluid inclusions in veins from the shear zones of the Kettara mafic ultra-mafic intrusion. (a-b) Tm(ice) (a) and Th (b) of primary (I) and secondary (II) aqueous saline fluid inclusions (type 3). (c-d) Tm(ice)) (c) and Th (d) of aqueous fluid inclusions (type 5). Vqcl : quartz-chlorite veins, Vqcc: quartz-calcite vein. * indicates the measures collected in calcite.

Fig. 12 Photomicrographs of fluid inclusions in mineralized veins of massive sulfide in transmitted light. A) quartz±carbonates mineralized vein: assemblage of two phase H2O-N2-CO2-CH4 inclusions (type 1) and one phase CH4-N2-CO2 inclusions (type 2). (B-E) quartz-chlorite mineralized vein, B) Two phase aqueous fluid inclusions showing a thin tip in crystal growth direction of quartz (type 3), C) two phases H2O-CH4-(Salt) fluid inclusions in quartz wrapped by sulfides (type 4, figure 3f), D) one phase N2-CH4 fluid inclusions (type 5). E) Secondary plan of one phase CH4 fluid inclusions (type 6).

Fig. 13 Histogram frequency of microthermometric data of fluid inclusions in mineralized veins of the Kettaramassive sulfide. (a-b)Tm(ice) (A) and Th (B) of aqueous gas-bearing fluid inclusions (type 1 and 4). (C-D)Th of gas-rich fluid inclusions (type 2, 5 and 6). (E-F) Tm(ice) (E) and Th (F) of aqueous fluid inclusions (type 3). Homogenization occurs into liquid phase (l) or vapor phase (v). Vm-qc: quartz±carbonates mineralized vein, Vm-qcl : quartz-chlorite mineralized vein.

Fig. 14 Ternary diagram showing the repartition of gas phases in fluid inclusions of the mineralized veins of the Kettara massive sulfidedeposit and the veins of the shear zones inthe Kettara intrusion. A) Aqueous gas-bearing inclusions ((H2O-gas-(Salt)), type 1 and type 4 of all veins) showing a sparse repartition of gases. B) Gas-rich fluid inclusions (type 2 of all veins and type 5 and type 6 in mineralized veins) showing the prevalence of CH_4 and N_2 in the mineralized veins and CO_2 in the veins associated tothe shear zones of the intrusion.

Fig. 15 Plot in $T_h$vs$T_{m(ice)}$ binary diagram of representative microthermometric data of type 1,type 3, type 4 and type 5 fluid inclusions of the veins associated tothe shear zones of the Kettara intrusion (see description in the text).

TABLE 1. oxygen (δ18O) and hydrogen (δD) isotope composition of chlorite and quartz of the Kettara deposit, the mineralized veins and the shear zones of the Kettara intrusion

			chlorite		Quartz
Location	**Lithology**	**Sample**	**$\delta^{18}O$ (‰)**	**δD (‰)**	**$\delta^{18}O$ (‰)**
Kettara deposit	Massive pyrhotite	KET5	6.24	-48	
Kettara deposit	Mineralized vein	KIM7-2	7.8	-52	9.1
Kettara intrusion	Quartz-chlorite vein	KTG2	4.4	-52	9.8
Kettara intrusion	Chlorite schist[1]	MK3	6.01		

[1]from Essaifi et al. (2004)

TABLE 2. Summary of microthermometric and Raman spectrometric data of fluid inclusions in mineralized veins of the Kettara massive sulfide deposit and in veins associated with shear zones of the Kettara mafic-ultra mafic intrusion

A-Kettara deposit

Fluid inclusion type	Range	$T_{h(gas)(l)}$ °C	$T_{h(gas)(v)}$ °C	$T_{m(CO2)}$ °C	$T_{m(ice)}$ °C	$T_{m(cl)}$ °C	$T_{h(CO2)(l)}$ °C	$T_{h(CO2)(v)}$ °C	$T_{h(l)}$ °C	$T_{h(c)}$ °C	**Td** °C	**Salinity** wt% NaCl	R_{flv} %	**Size** µm	CO_2 %	N_2 %	CH_4 %	**Others**
Quartz-carbonates mineralized vein (Vm-qc)																		
Type 1	Minimum				-9.1	2.9			178				5	5	8.7	0.0	8.4	
$H_2O-CO_2-N_2-CH_4$	Maximum				0.0	10.1			230				10	50	84.1	79.0	51.7	
	Average				-3.6	6.2			210				5	17	44.0	34.4	21.7	
	N[3]				18	6			15				18	18	8	8	8	
Type 2	Minimum	-99.4	-95.9											5	11.5	21.0	36.1	
$CH_4-N_2-CO_2$	Maximum	-70.4	-78.3											20	27.0	38.1	67.5	
	Average	-91.4	-88.9											11	20.0	31.9	48.0	
	N	4	5											9	7	7	7	
Type 3	Minimum				-7.9				176			3.4	5	5				
H_2O	Maximum				-2.0				258			11.6	20	30				
	Average				-4.7				223			7.4	7	11				
	Numer of data				37				32			24	50	50				
Quartz-chlorite mineralized vein (Vm-qcl)																		
Type 3	Minimum				-17.4				174			1.1	5	5				
H_2O	Maximum				-0.6				260			20.5	10	20				
	Average				-6.3				218			9.1	7	9				
	N				43				11			43	42	41				
Type 4	Minimum				-19.2	5.8			212				5	5			100	graphite
H_2O-CH_4	Maximum				-0.3	11			376				20	20			100	
	Average				-6.0	8.6			291				10	10			100	
	N				14	4			15				17	17			5	1
Type 5	Minimum	-121.7	-124.1											5		49.8	39.6	
N_2-CH_4	Maximum	-121.7	-105.2											18		60.4	50.2	
	Average	-121.7	-118.5											12		55.5	44.5	
	Numer of	1	10											9		6	6	
Type 6	Minimum	-97.4	-85.5											5			100	graphite
CH_4	Maximum	-93.4	-82											20			100	
	Average	-96	-85											11			100	
	N	4	9											13			14	1

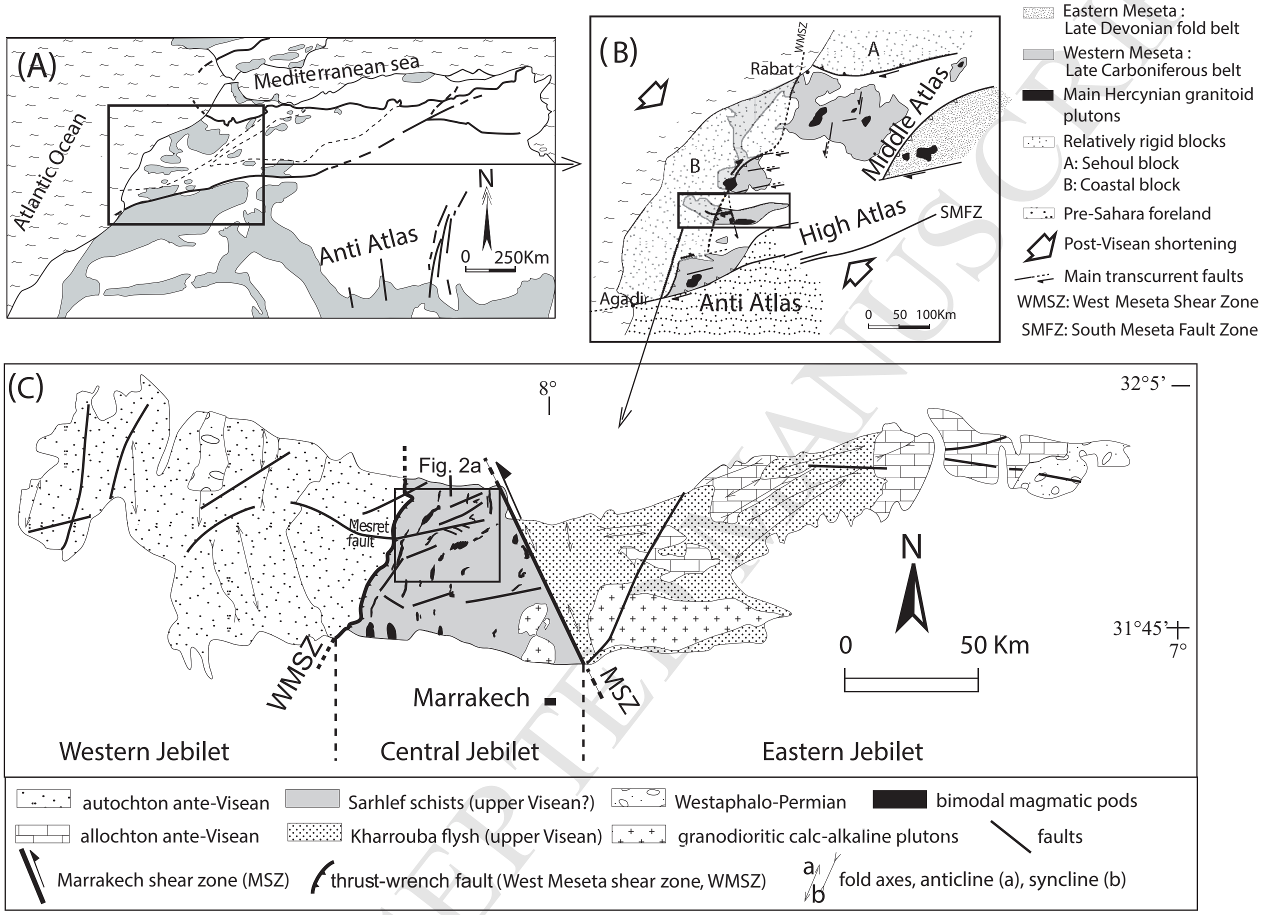
(A)
Mediterranean sea
Atlantic Ocean
Anti Atlas
N
0 250Km
(B)
Rabat
WMSZ
A
B
Middle Atlas
High Atlas
SMFZ
Agadir
Anti Atlas
0 50 100Km
Eastern Meseta : Late Devonian fold belt
Western Meseta : Late Carboniferous belt
Main Hercynian granitoid plutons
Relatively rigid blocks
A: Sehoul block
B: Coastal block
Pre-Sahara foreland
Post-Visean shortening
Main transcurrent faults
WMSZ: West Meseta Shear Zone
SMFZ: South Meseta Fault Zone
(C)
8°
32°5’
Fig. 2a
Mesret fault
N
0 50 Km
31°45’
7°
WMSZ
Marrakech
MSZ
Western Jebilet
Central Jebilet
Eastern Jebilet
autochton ante-Visean
Sarhlef schists (upper Visean?)
Westaphalo-Permian
bimodal magmatic pods
allochton ante-Visean
Kharrouba flysh (upper Visean)
granodioritic calc-alkaline plutons
faults
Marrakech shear zone (MSZ)
thrust-wrench fault (West Meseta shear zone, WMSZ)
fold axes, anticline (a), syncline (b)

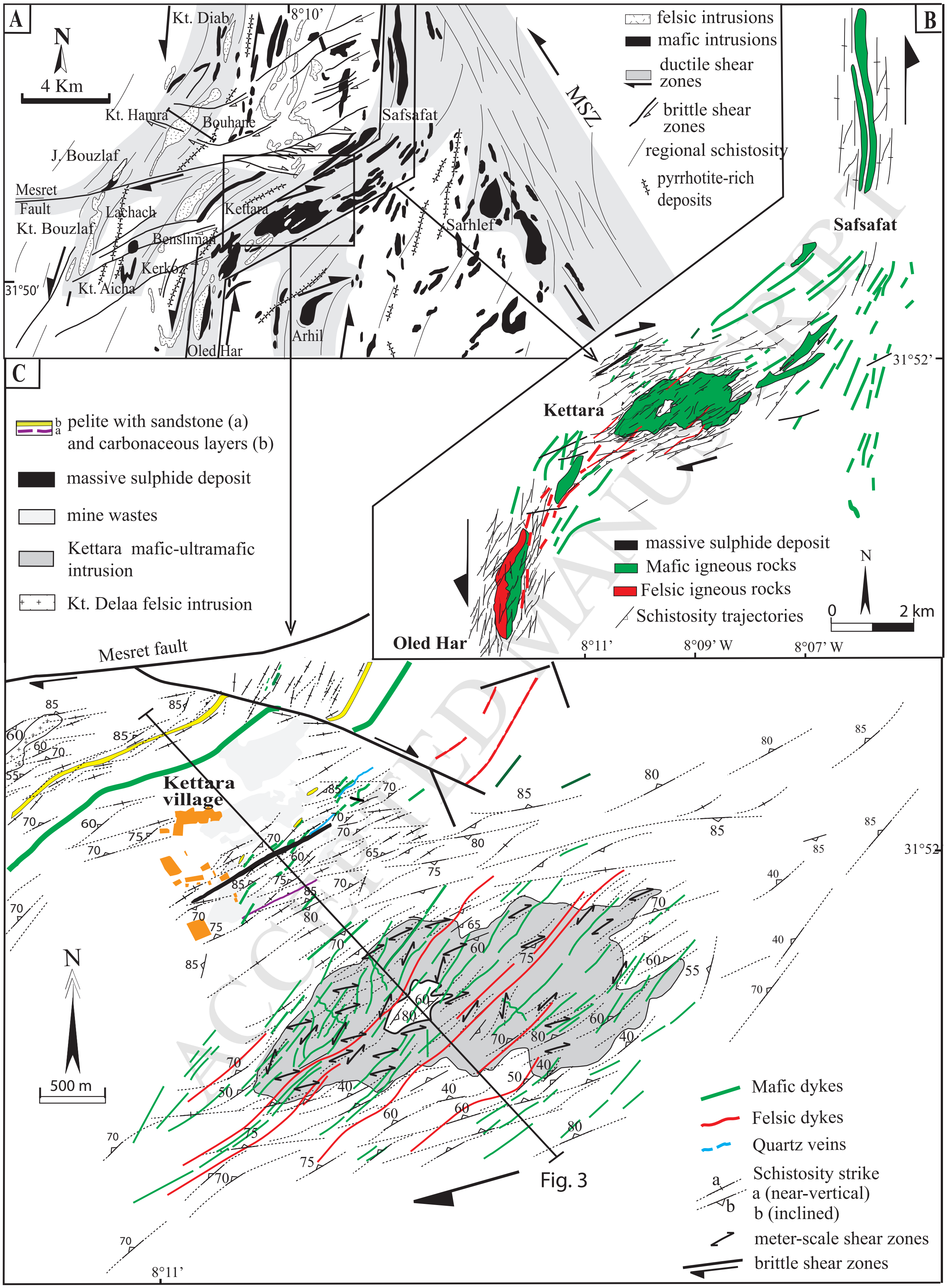

A
N
4 Km
Kt. Diab
8°10'
Kt. Hamra
Bouhane
Safsafat
MSZ
J. Bouzlaf
Mesret
Fault
Kt. Bouzlaf
Lachach
Keftara
Benslimane
Kerkor
Kt. Aicha
Sarhlef
31°50'
Oled Har
Arhil
felsic intrusions
mafic intrusions
ductile shear zones
brittle shear zones
regional schistosity
pyrrhotite-rich deposits
B
Safsafat
31°52'
Kettara
Oled Har
massive sulphide deposit
Mafic igneous rocks
Felsic igneous rocks
Schistosity trajectories
N
0
2 km
8°11'
8°09' W
8°07' W
C
pelite with sandstone (a)
and carbonaceous layers (b)
massive sulphide deposit
mine wastes
Kettara mafic-ultramafic intrusion
Kt. Delaa felsic intrusion
Mesret fault
Kettara village
N
500 m
31°52'
Fig. 3
Mafic dykes
Felsic dykes
Quartz veins
Schistosity strike
a (near-vertical)
b (inclined)
meter-scale shear zones
brittle shear zones
8°11'

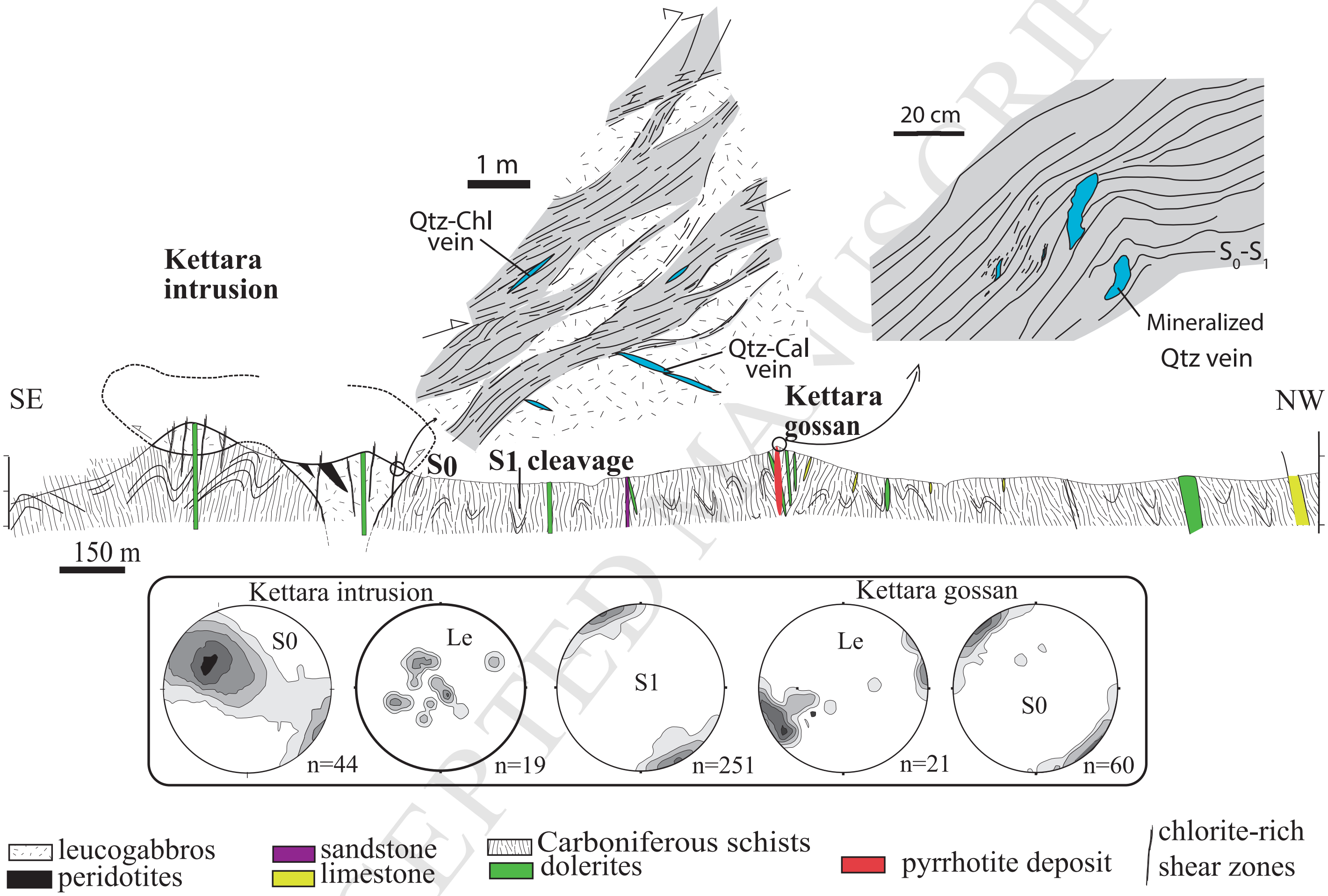

Kettara intrusion
1 m
Qtz-Chl vein
Qtz-Cal vein
20 cm
S0-S1
Mineralized Qtz vein
SE
NW
Kettara gossan
S0
S1 cleavage
150 m
Kettara intrusion
S0
n=44
Le
n=19
S1
n=251
Kettara gossan
Le
n=21
S0
n=60
leucogabbros
peridotites
sandstone
limestone
Carboniferous schists
dolerites
pyrrhotite deposit
chlorite-rich shear zones

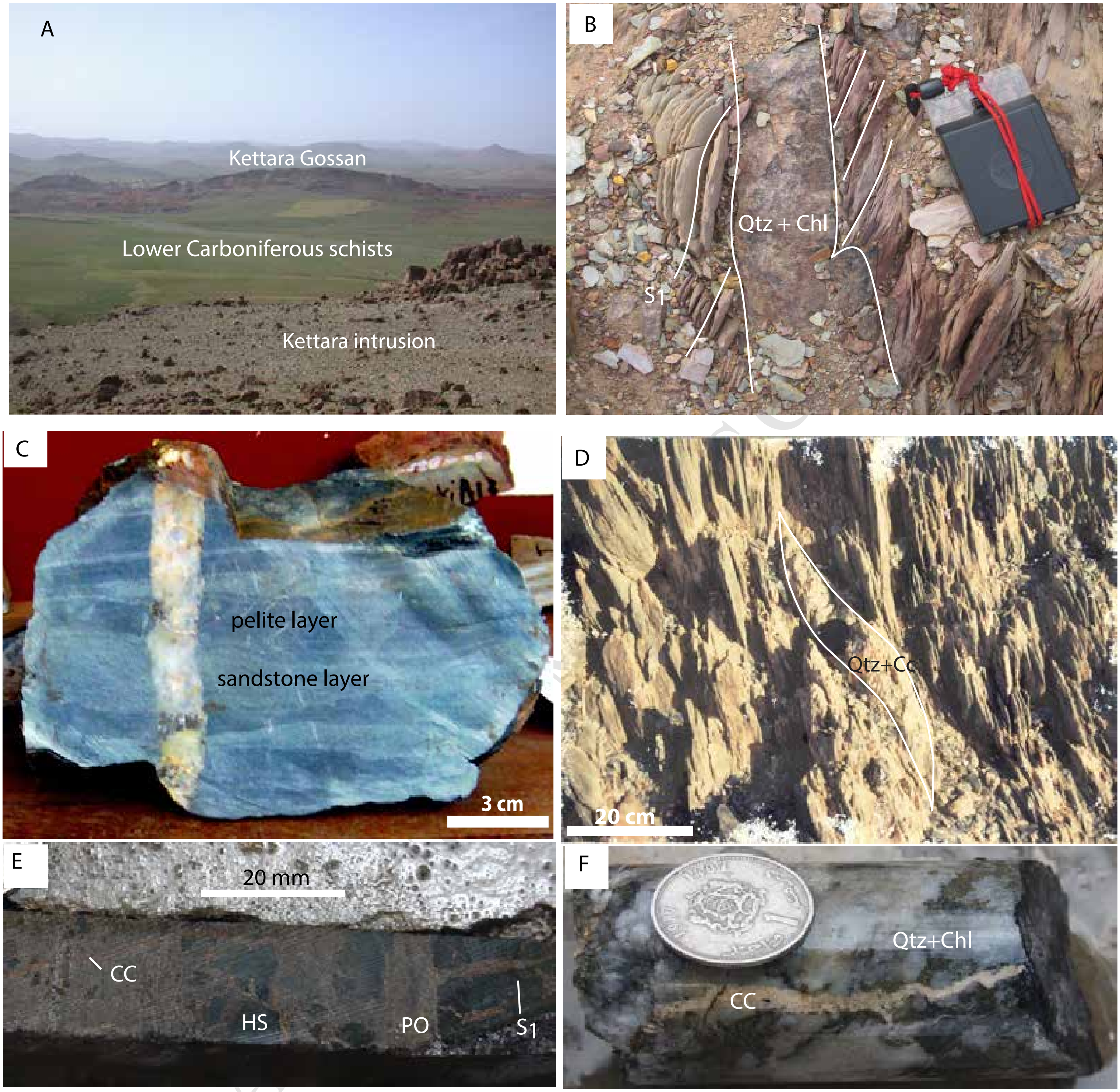
A
Kettara Gossan
Lower Carboniferous schists
Kettara intrusion
B
Qtz + Chl
S1
C
pelite layer
sandstone layer
3 cm
D
Qtz+Cc
20 cm
E
20 mm
CC
HS
PO
S1
F
Qtz+Chl
CC

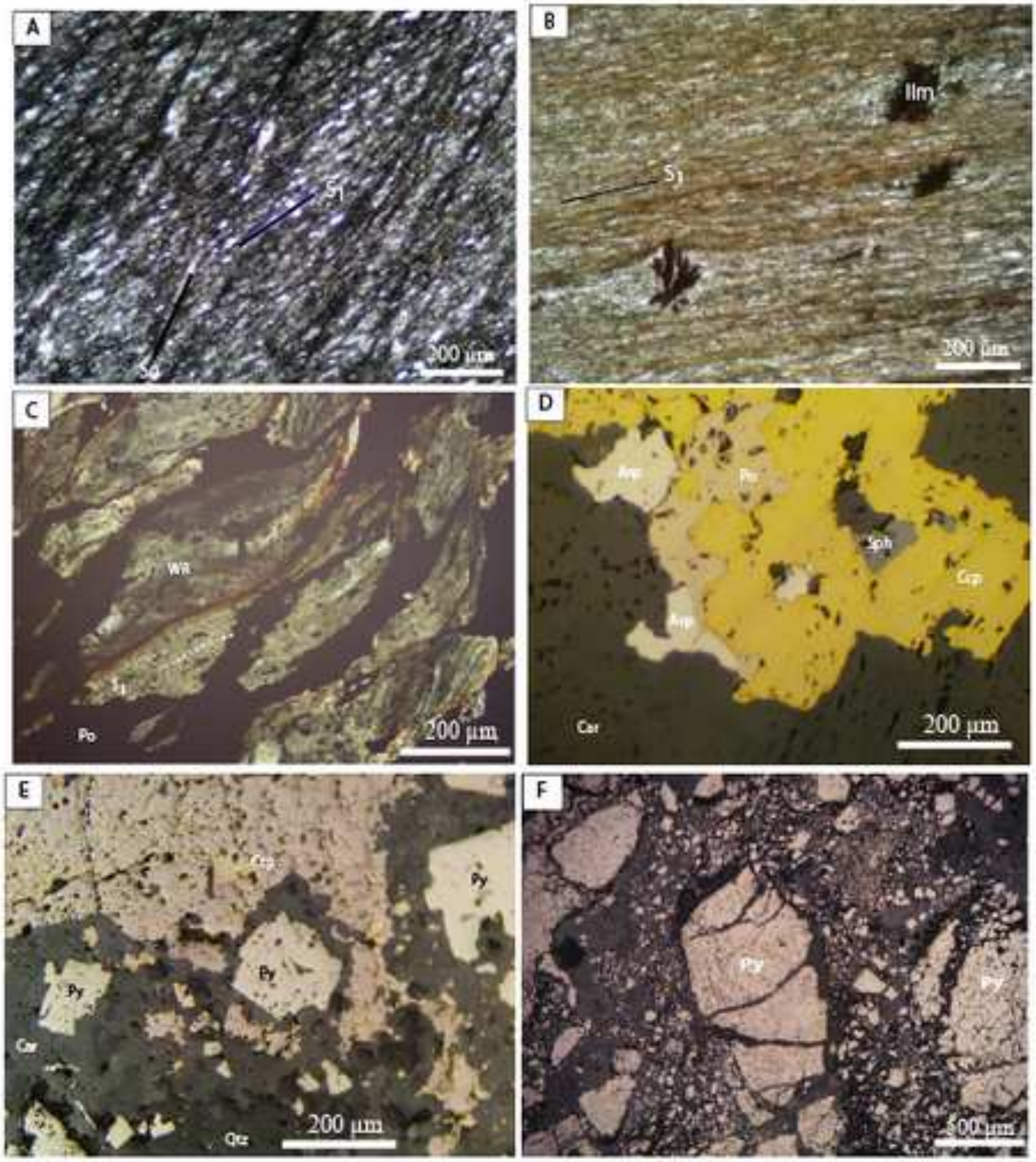
A
S1
S0
200 µm
B
Ilm
S1
200 µm
C
WR
S1
Po
200 µm
D
Apy
Po
Sph
Ccp
Car
200 µm
E
Ccp
Py
Py
Py
Car
Qtz
200 µm
F
Py
Py
500 µm

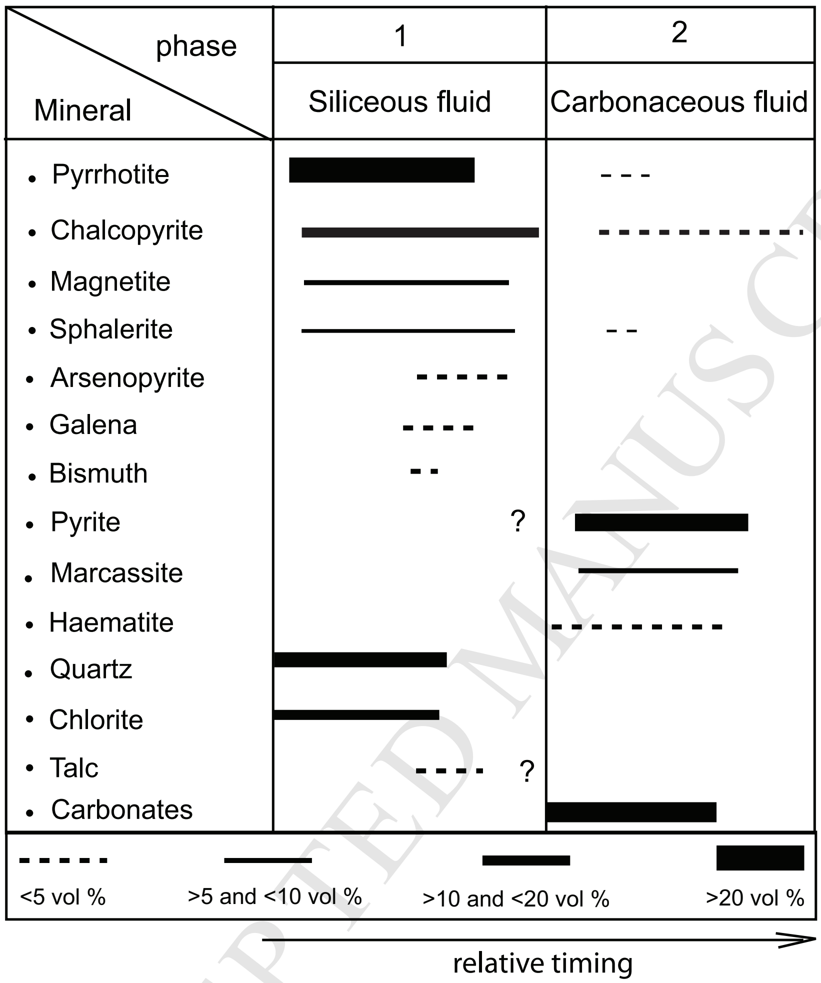
phase
Mineral
1
2
Siliceous fluid
Carbonaceous fluid
Pyrrhotite
Chalcopyrite
Magnetite
Sphalerite
Arsenopyrite
Galena
Bismuth
Pyrite
Marcassite
Haematite
Quartz
Chlorite
Talc
Carbonates
?
?
<5 vol %
>5 and <10 vol %
>10 and <20 vol %
>20 vol %
relative timing

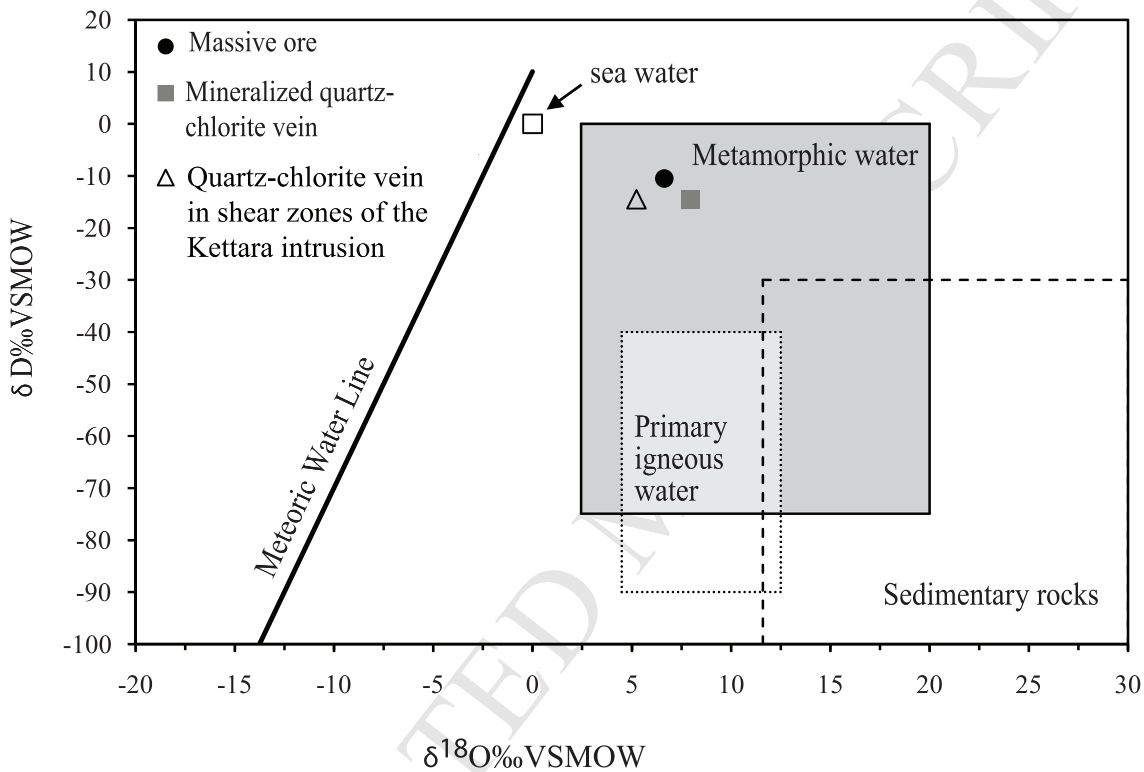
Massive ore
Mineralized quartz-chlorite vein
Quartz-chlorite vein in shear zones of the Kettara intrusion
sea water
Metamorphic water
Meteoric Water Line
Primary igneous water
Sedimentary rocks
δ D‰VSMOW
δ18O‰VSMOW
20
10
0
-10
-20
-30
-40
-50
-60
-70
-80
-90
-100
-20
-15
-10
-5
0
5
10
15
20
25
30

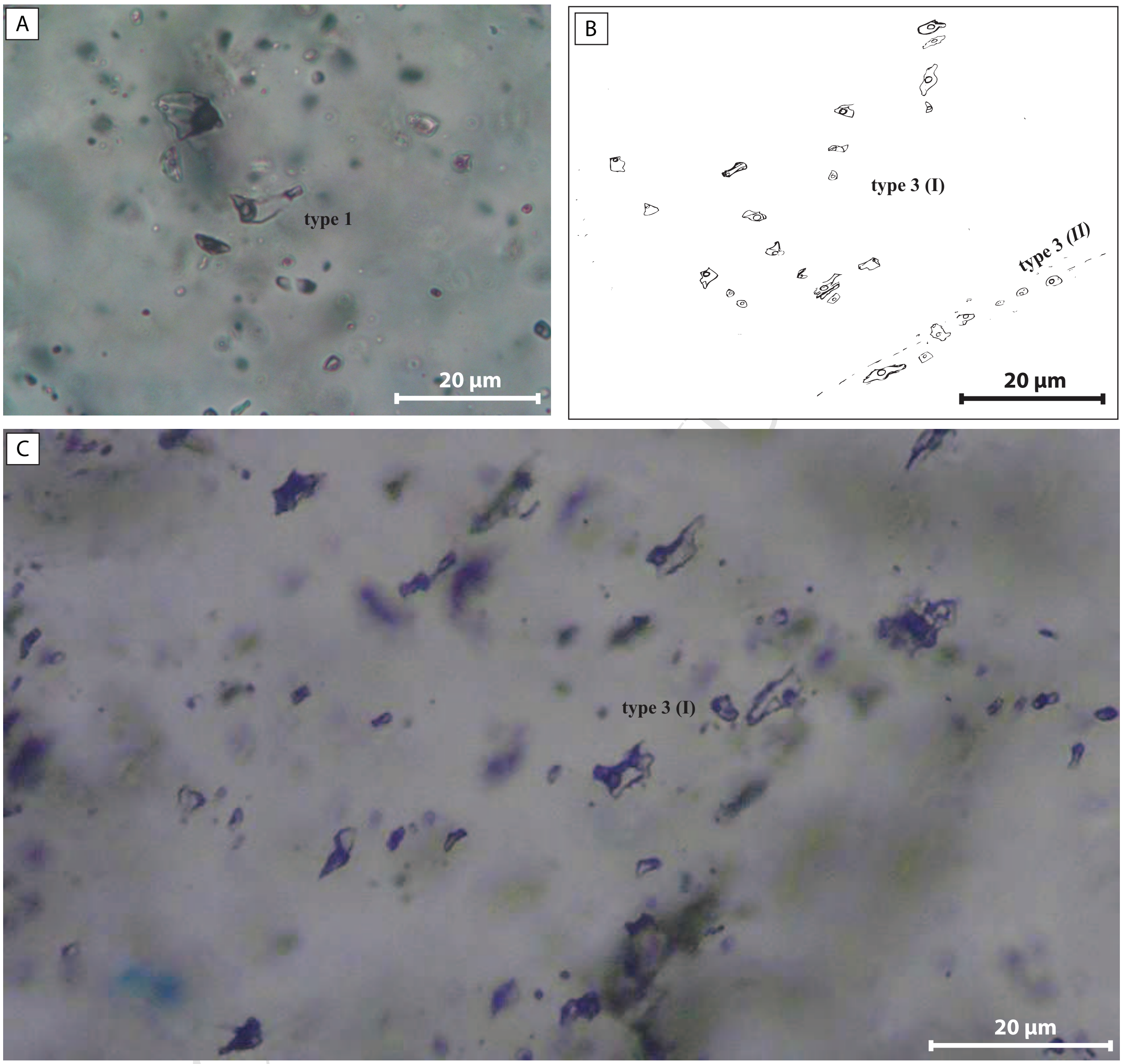
A
type 1
20 µm
B
type 3 (I)
type 3 (II)
20 µm
C
type 3 (I)
20 µm

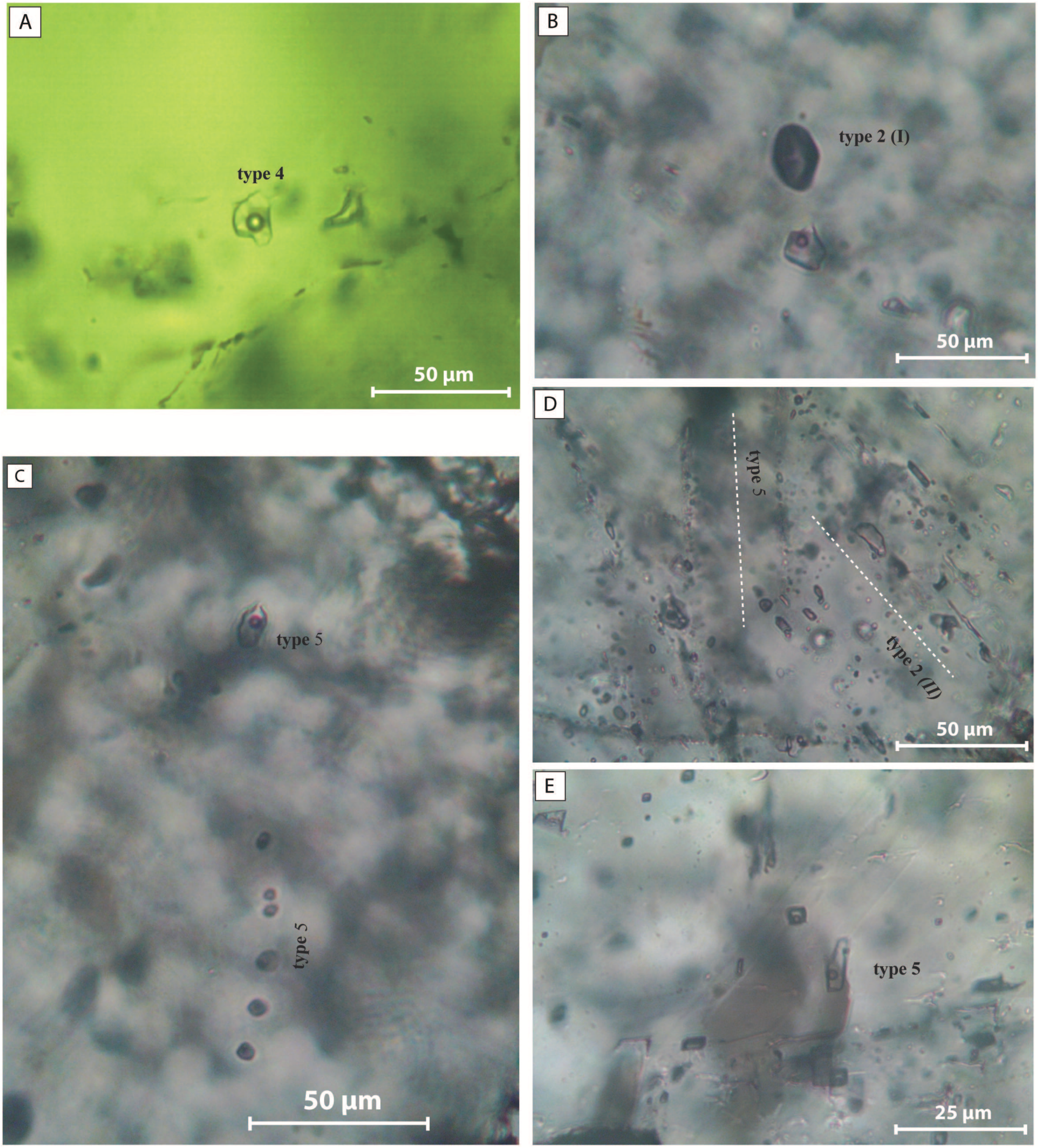
A
type 4
50 µm
B
type 2 (I)
50 µm
C
type 5
type 5
50 µm
D
type 5
type 2 (II)
50 µm
E
type 5
25 µm

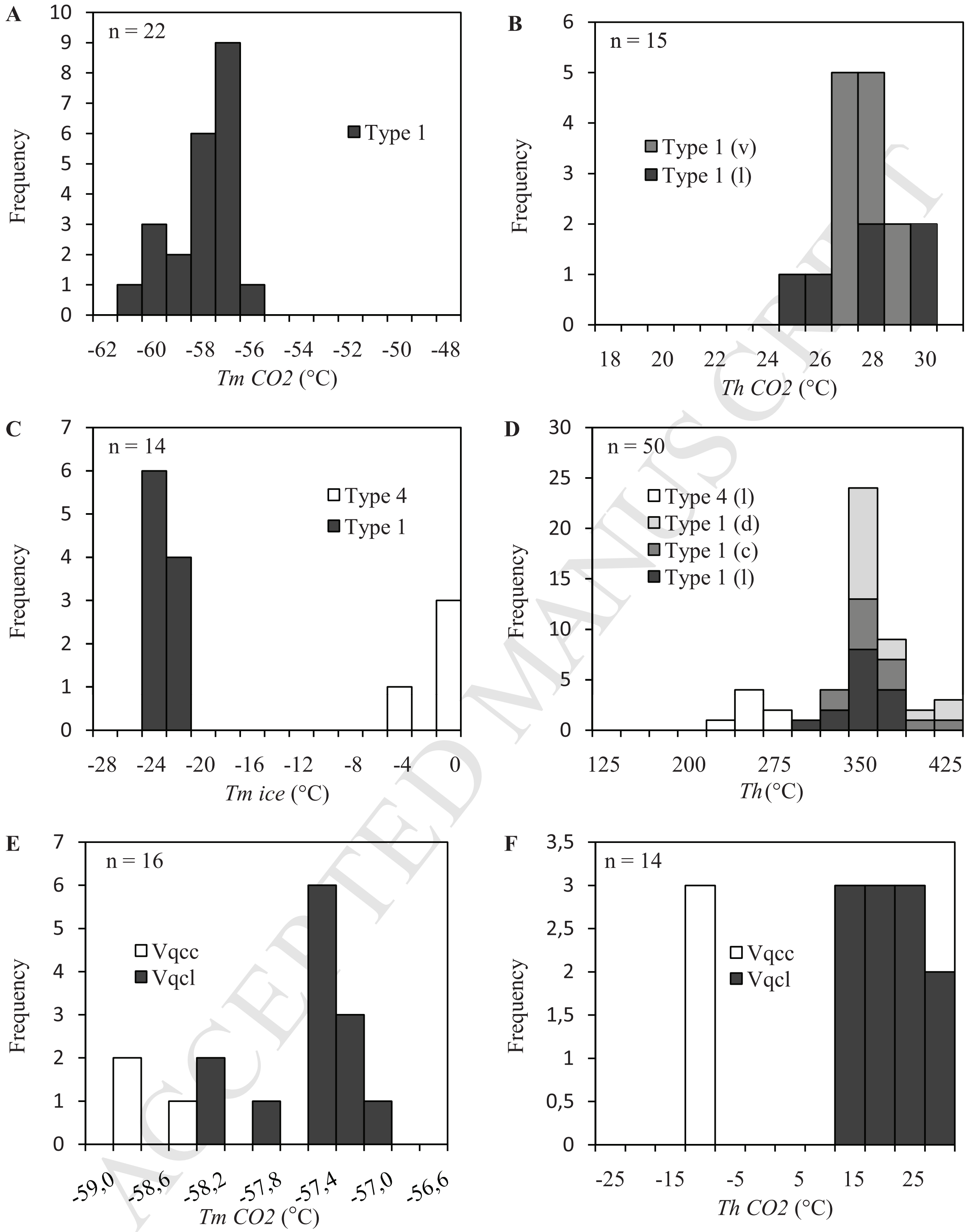
A
n = 22
Type 1
Frequency
Tm CO2 (°C)
B
n = 15
Type 1 (v)
Type 1 (l)
Frequency
Th CO2 (°C)
C
n = 14
Type 4
Type 1
Frequency
Tm ice (°C)
D
n = 50
Type 4 (l)
Type 1 (d)
Type 1 (c)
Type 1 (l)
Frequency
Th (°C)
E
n = 16
Vqcc
Vqcl
Frequency
Tm CO2 (°C)
F
n = 14
Vqcc
Vqcl
Frequency
Th CO2 (°C)

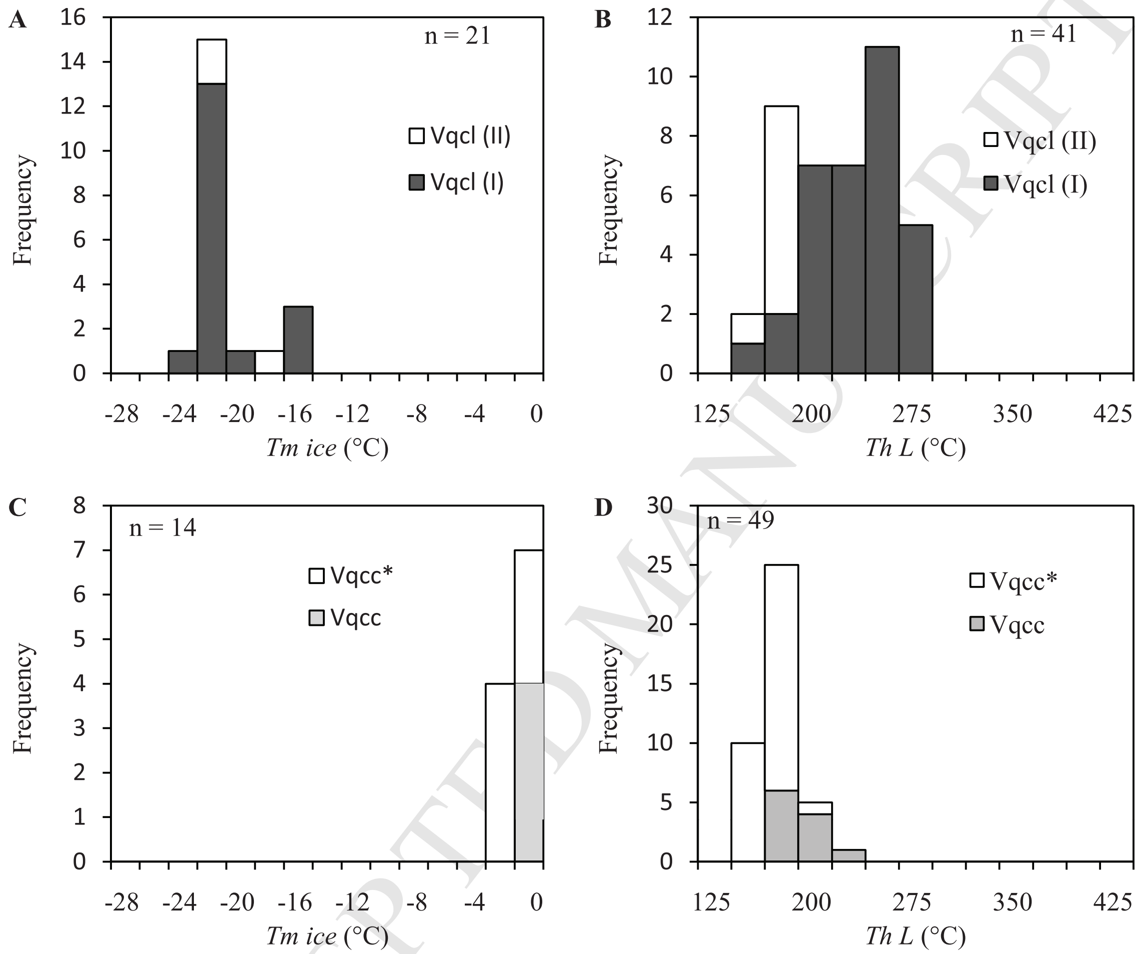
A
n = 21
Vqcl (II)
Vqcl (I)
Frequency
Tm ice (°C)
B
n = 41
Vqcl (II)
Vqcl (I)
Frequency
Th L (°C)
C
n = 14
Vqcc*
Vqcc
Frequency
Tm ice (°C)
D
n = 49
Vqcc*
Vqcc
Frequency
Th L (°C)

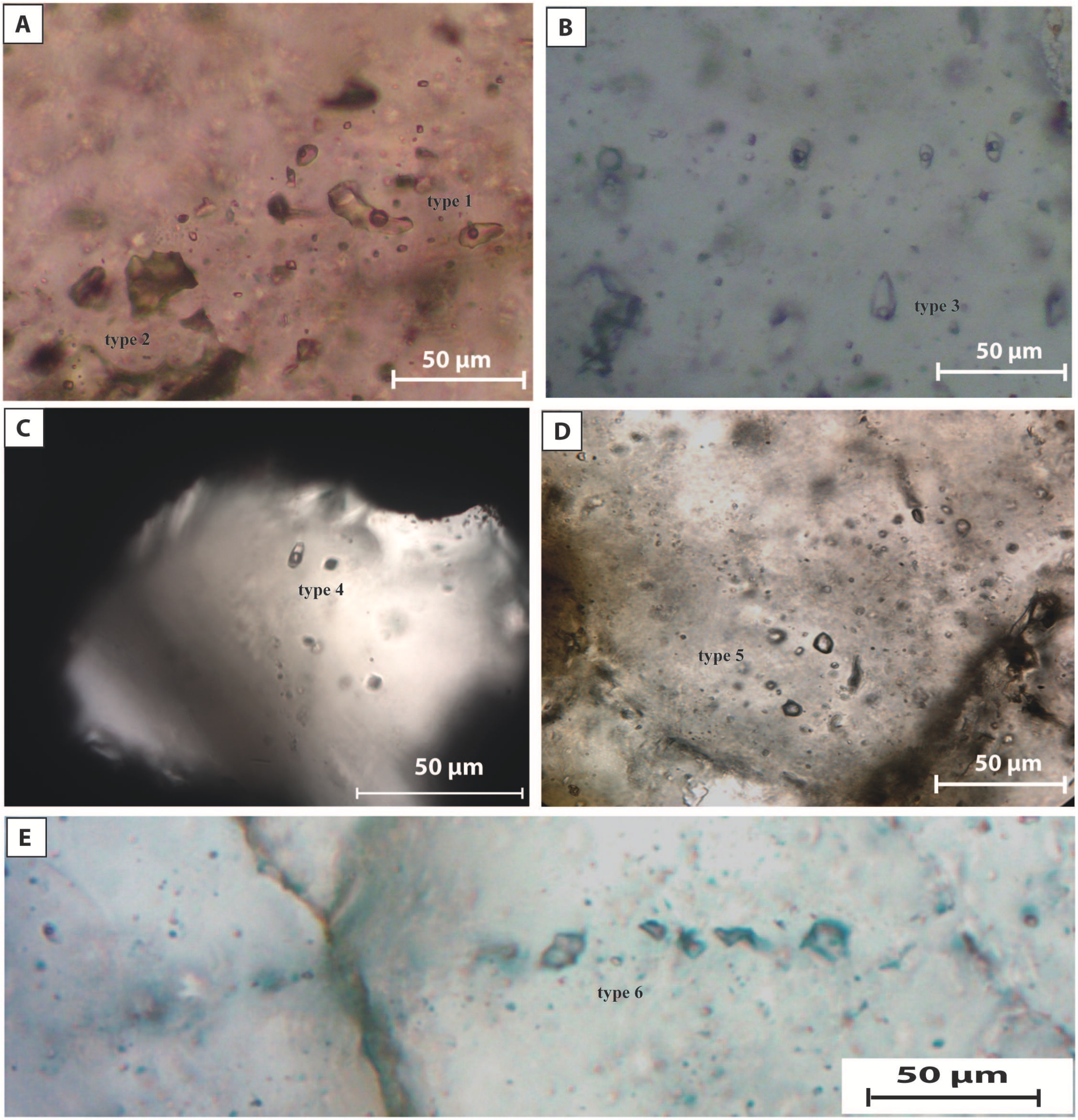
A
type 1
type 2
50 µm
B
type 3
50 µm
C
type 4
50 µm
D
type 5
50 µm
E
type 6
50 µm

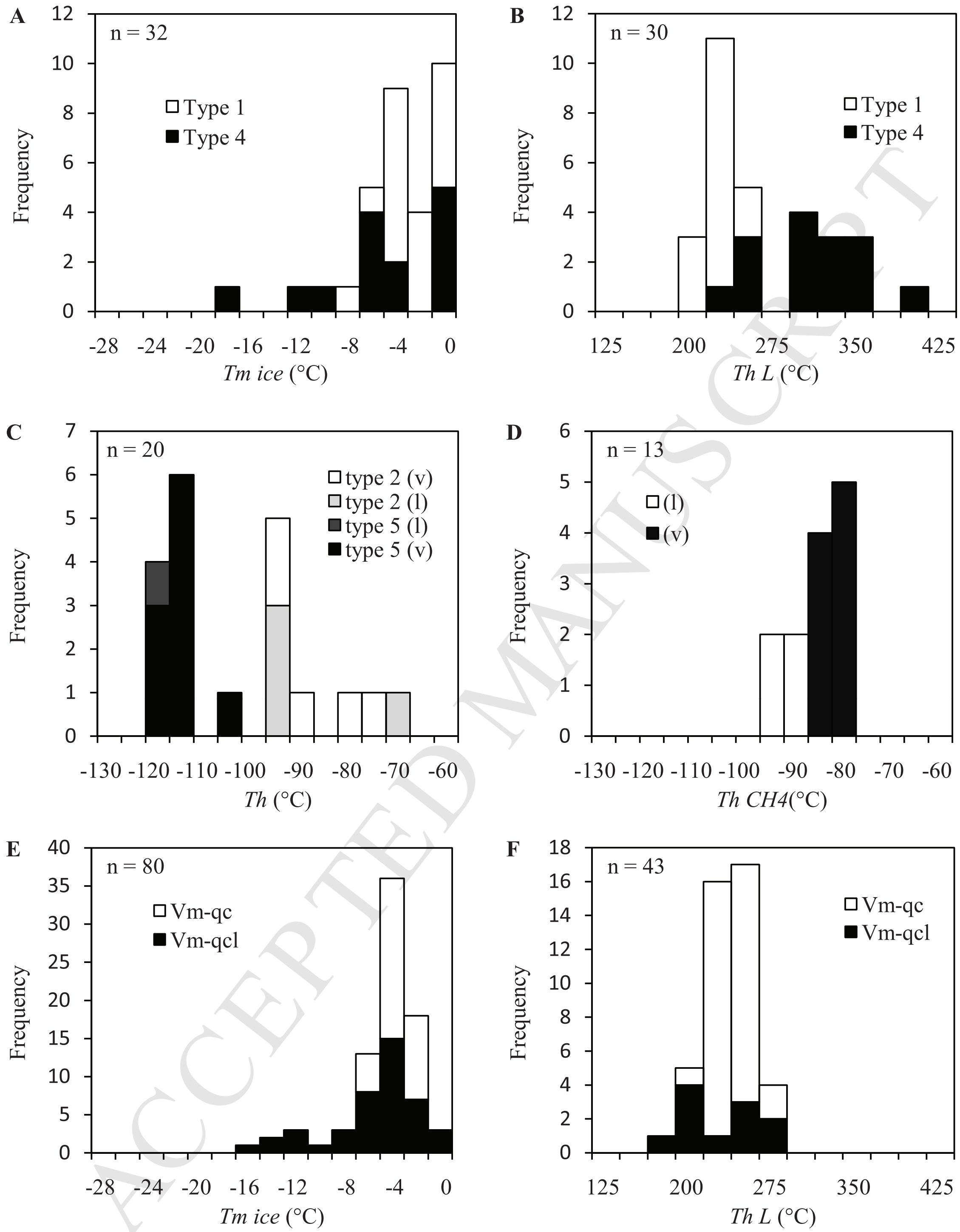
A
n = 32
Type 1
Type 4
Frequency
Tm ice (°C)
B
n = 30
Type 1
Type 4
Frequency
Th L (°C)
C
n = 20
type 2 (v)
type 2 (l)
type 5 (l)
type 5 (v)
Frequency
Th (°C)
D
n = 13
(l)
(v)
Frequency
Th CH4(°C)
E
n = 80
Vm-qc
Vm-qcl
Frequency
Tm ice (°C)
F
n = 43
Vm-qc
Vm-qcl
Frequency
Th L (°C)

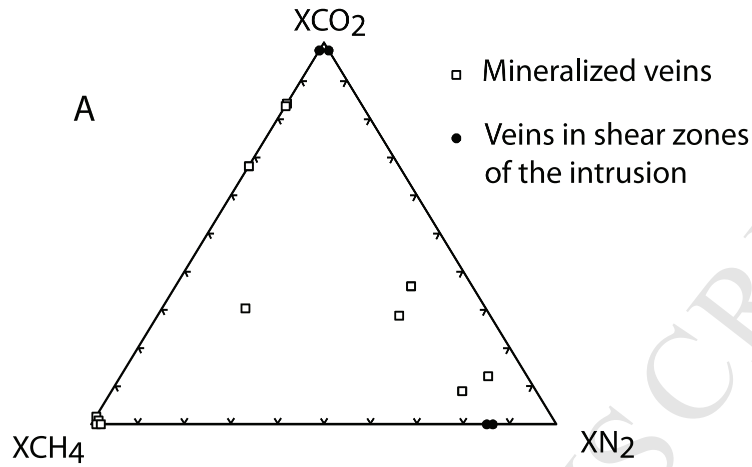
XCO2
A
Mineralized veins
Veins in shear zones
of the intrusion
XCH4
XN2

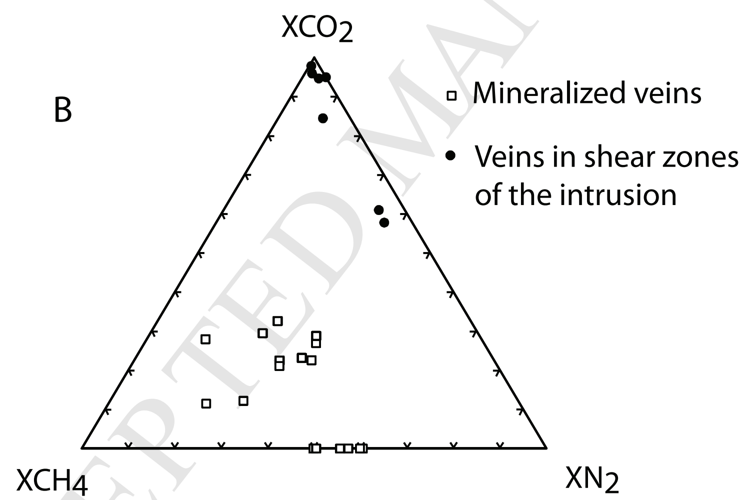
XCO2
B
Mineralized veins
Veins in shear zones
of the intrusion
XCH4
XN2

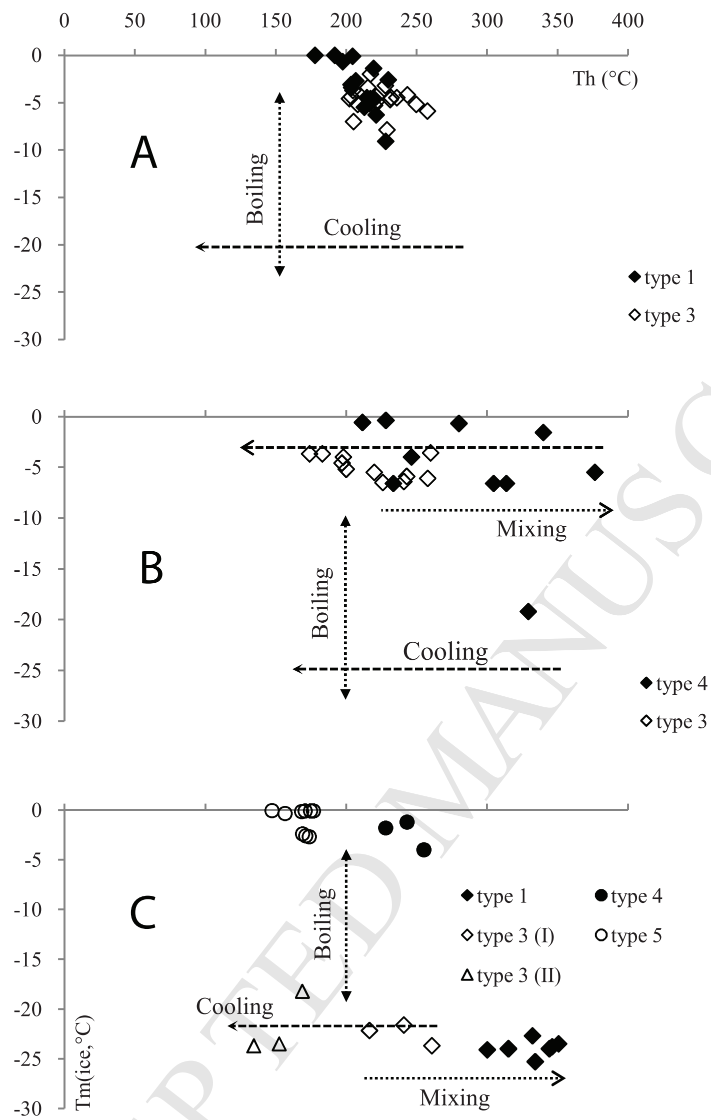

Th (°C)
A
Boiling
Cooling
type 1
type 3
B
Mixing
Boiling
Cooling
type 4
type 3
C
Boiling
Cooling
Mixing
type 1
type 4
type 3 (I)
type 5
type 3 (II)
Tm(ice,°C)

Highlights:

Kettara shear zone hosts a mafic-ultramafic intrusion and a Cu-deposit

A regional metamorphic fluid flow occurred through the shear zone

Reduction of fluids induced sulfides precipitation in wall rocks of the deposit